

Article

Analysis of Factors Driving Subtropical Forest Phenology Differentiation, Considering Temperature and Precipitation Time-Lag Effects: A Case Study of Fujian Province

Menglu Ma ^{1,2}, Hao Zhang ^{1,2}, Jushuang Qin ^{1,2}, Yutian Liu ^{1,2}, Baoguo Wu ^{1,3}  and Xiaohui Su ^{1,2,*} 

¹ School of Information Science and Technology, Beijing Forestry University, Beijing 100083, China; maml1116@bjfu.edu.cn (M.M.); haozhang@bjfu.edu.cn (H.Z.); qinjs123@bjfu.edu.cn (J.Q.); lyt7230434@bjfu.edu.cn (Y.L.); wubg@bjfu.edu.cn (B.W.)

² Engineering Research Center for Forestry-Oriented Intelligent Information Processing, National Forestry and Grassland Administration, Beijing 100083, China

³ Research Institute of Forestry Informatization, Beijing Forestry University, Beijing 100083, China

* Correspondence: suxhui@bjfu.edu.cn

Abstract: Subtropical forest phenology differentiation is affected by temperature, precipitation, and topography. Understanding the primary contributing elements and their interactions with forest phenology can help people better comprehend the subtropical forest growth process and its response to climate. Meanwhile, the temporal and spatial variations of phenological rhythms are important indicators of climatic impacts on forests. Therefore, this study aimed to analyze both a total area and different forest growth environments within the whole (i.e., coastal site areas (II, IV) and inland site areas (I, III)) as to spatiotemporal patterns associated with subtropical forests in Fujian Province, which is located at the boundary between the middle and south subtropical zones. Considering the asymmetric effects of climate and forest growth, this study chose pre-seasonal and cumulative temperature and precipitation factors and utilized the GeoDetector model to analyze the dominant drivers and interactions within phenology differentiation in Fujian Province. The results show the following: (1) All of the phenological parameters were advanced or shortened over the 19-year observation period; those of shrubland and deciduous broadleaf forests fluctuated greatly, and their stability was poor. (2) The phenological parameters were more distinct at the borders of the site areas. Additionally, the dates associated with the end of the growth season (EOS) and the date-position of peak value (POP) in coastal areas (i.e., II and IV) were later than those in inland areas (i.e., I and III). Among the parameters, the length of the growth season (LOS) was most sensitive to altitude. (3) Precipitation was the main driving factor affecting the spatial heterogeneity of the start of the growth season (SOS) and the EOS. The relatively strong effects of pre-season and current-month temperatures on the SOS may be influenced by the temperature threshold required to break bud dormancy, and the relationship between the SOS and temperature was related to the lag time and the length of accumulation. The EOS was susceptible to the hydrothermal conditions of the pre-season accumulation, and the variation trend was negatively correlated with temperature and precipitation. Spatial attribution was used to analyze the attribution of phenology differentiation from the perspectives of different regions, thus revealing the relationships between forest phenology and meteorological time-lag effects, the result which can contribute to targeted guidance and support for scientific forest management.

Keywords: driving force; GeoDetector; MCD12Q2; subtropical forest phenology; time-lag effect



Citation: Ma, M.; Zhang, H.; Qin, J.; Liu, Y.; Wu, B.; Su, X. Analysis of Factors Driving Subtropical Forest Phenology Differentiation, Considering Temperature and Precipitation Time-Lag Effects: A Case Study of Fujian Province. *Forests* **2024**, *15*, 334. <https://doi.org/10.3390/f15020334>

Academic Editor: Wangping Li

Received: 26 December 2023

Revised: 6 February 2024

Accepted: 6 February 2024

Published: 8 February 2024



Copyright: © 2024 by the authors. Licensee MDPI, Basel, Switzerland. This article is an open access article distributed under the terms and conditions of the Creative Commons Attribution (CC BY) license (<https://creativecommons.org/licenses/by/4.0/>).

1. Introduction

Phenology refers to the growth and development rhythms of vegetation, such as sprouting, branching, leaf spreading, flowering, fruiting, leaf fall, and dormancy [1]. Under the effects of global climate change, the fluctuations of forest phenology can reflect the impact of

climate on terrestrial ecosystems [2]. It is vital to promptly understand the spatiotemporal characteristics of phenology to mitigate the negative effects of climate on forest growth [3]. With the development of remote-sensing technology, it is possible to observe phenology over a large area. Based on the vegetation index (VI) calculated from spectral information, the phenological extraction process can be summarized into two steps: (1) VI time series denoising and smoothing, in which the cloud and rain flags in the remote-sensing quality band are combined to remove the cloud from the VI time series, and then filtering or function fitting methods such as Savitzky–Golay [4], Asymmetric Gaussian [5], Double Logistic [6], and Whittaker [7] are used to denoise and smooth to obtain high-quality VI time series. (2) The extraction of phenological indicators then follows. According to the reconstructed time series, phenological extraction methods such as the threshold methods (e.g., dynamic threshold method [8]) and the VI change monitoring methods (e.g., moving-average method [9]) are used to obtain the characteristic nodes of key phenological stages such as the start of the growth season (SOS), the end of the growth season (EOS), the length of the growth season (LOS), and the date-position of peak value (POP). Recent phenological studies based on remote-sensing observation have mainly concentrated on middle and high latitudes [10,11], temperate-zone regions [12,13], and regions vulnerable to climate change [3,14]; in contrast, relatively few studies have focused on subtropical and low latitudes with complex stand structures and diverse phenological patterns. East Asian subtropical forests account for approximately 8% of the global net ecosystem productivity and have gradually become an important ecological-function area for investigations into the mitigation of global warming [15,16]. As the area with the highest subtropical-forest coverage rate in China [17], Fujian Province plays an important role in the ecological balance. Moreover, it is located on the transition zone between the middle and the south subtropical zones, and has different soil types and climate conditions [18]. The LOS, which is derived by subtracting the ending and starting periods of the growth season, affects the net primary productivity of forests and the carbon balance of terrestrial ecosystems [19,20]. Therefore, to help design effective methods for the management of forests and improve the quality of those managed forests, it is beneficial to understand the spatiotemporal patterns and change-related trends of subtropical forest phenology, as well as the driving forces and importance factors of leading their spatial heterogeneity. The findings of these investigations can be used to improve the productivity of subtropical forests in Fujian Province.

Phenological parameters, especially the driving mechanisms of spatial differentiation between SOS and EOS, are the key to reflecting the relationship between tree growth and the surrounding environment. Among meteorological factors, temperature and precipitation have the greatest influence on changes in vegetation phenology [21,22], as hydrothermal conditions regulate current and subsequent forest growth. For example, the heat- and cold-accumulation temperatures of trees before the SOS are related to the beginning of tree leaf growth [23,24]. Deciduous forests have obvious leaf-falling and germination phenomena. The phenology of evergreen forests is primarily represented by the alternating growth of new and old leaves [25]. In addition, there is a dormant phase preceding leaf germination, during which low temperatures are required to transition the dormant bud from the ecodormancy to endodormancy period, just as in deciduous forests [24,26]. Previous studies have usually used traditional statistical methods, such as correlation, regression, distributed lag regression models, or vector autoregressive models, to analyze the time-lag effects [22,27–29], and these results have indicated the sensitivity of the vegetation growth to a single pre-season meteorological factor. However, the explanation of phenological spatial differentiation by use of multiple climatic factors is stronger than that by a single climatic factor [30]. A multi-level analysis of the comprehensive effects of climate, topographic features, and forest types is of profound significance for understanding the driving mechanisms of phenological spatial differentiation. The geographical distribution relationship is often overlooked, even though the usual multiple-regression approach may be used to evaluate the level of phenological differentiation of various components. It is

generally difficult to specify the effect-intensity and interaction between factors in different regions, and the degrees of the effects of both single and combined factors on phenological differentiation are lacking.

GeoDetector analyzed the differences between within-strata variances and between-strata variances to quantify the relative influence of multiple potential drivers behind spatial heterogeneity. This was mainly to compare the consistency of the spatial distribution of the driving factors and the independent variables [31]. On the one hand, GeoDetector is a statistical model considering spatial non-stationarity. It can provide a way to explore the driving forces between driving factors and dependent variables from a geographical perspective. Importantly, this model can not only quantify the main potential driving factors but also detect the interactions between different driving factors for spatial heterogeneity [32]. On the other hand, the statistical method of the model is not affected by the multivariate collinearity effect, and the modeling process does not involve complex parameter settings or hypothesis constraints, which can more accurately describe the role and intensity of the influencing factors [32,33]. In the past, GeoDetector was used to study the asymmetric effects of climate and phenology, for which monthly and annual data were chosen as the driving factors of time lag [34–37]; however, the differences between pixels in the beginning and end months of phenology were ignored. Furthermore, the division of the research area did not account for the growing environment of vegetation and forest. Trees differ in their growth habits and status, as well as the terrain and soil in which they grow. According to the comprehensive action of natural environmental factors, the forest area can be rationally distributed, and the forest production and management objectives can be improved by understanding the relationship between the phenological changes and the climate in each area.

This study evaluates the spatiotemporal patterns of phenology and its environmental drivers in Fujian Province, China, by integrating spatial datasets of phenology, meteorology, and land cover. Specifically, the objectives are (1) to reveal the spatiotemporal differences in phenology in different regions and for different forest types in Fujian Province from 2001 to 2019, and (2) to explore the relationships between the meteorological lag effect, topographic factors, and the spatial heterogeneity of the SOS and EOS, while assessing the impacts of the geographical environment and climate on phenology. The findings provide scientifically informed recommendations to aid in forest planning and design, effectively addressing the challenges posed by global climate change, and enhancing forest productivity.

2. Materials and Methods

2.1. Study Area

Fujian Province is located in southeast China. The terrain is generally high in the northwest and low in the southeast, and is dominated by mountains and hills; Jiufeng Mountain, Daiyun Mountain, and Bopingling Mountain are located in the center, and Wuyi Mountain is located in the west. Fujian Province spans the central and south subtropical zones, and the precipitation is uneven between years and seasons due to the effects of the complex terrain. Therefore, as shown in Figure 1a, the forest growth environment can be divided into four regions according to different site conditions [38], namely, the mountainous region of Wuyi Mountain (I), the coastal low mountain and hill region of Zhejiang and Fujian (II), the mountainous and hill region of Jiangxi, Fujian, and Guangdong (III), and the coastal hill and plain region of Fujian and Guangdong (IV). According to the temperature zone division in the China eco-geographical regionalization [39], Fujian province spans the middle subtropical zone and the southern subtropical zone. The location of this division line is close to the boundary of region IV. Among these divisions, region IV is located in the south subtropical zone, while the other three regions are located in the middle subtropical zone. Fujian Province is abundant in forest resources, the majority of which are evergreen needleleaf forests and evergreen broadleaf forests.

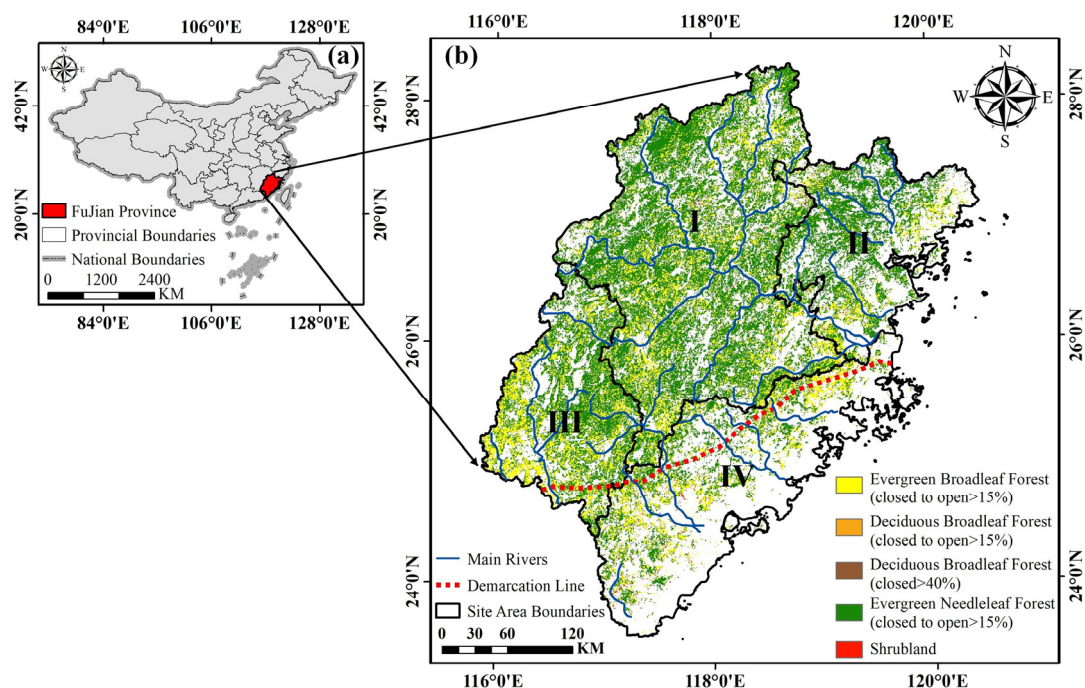


Figure 1. The geographical location of the study area: (a) the geographical location of the study area in China; (b) the distribution of forest type, site area, demarcation line, and main rivers in Fujian Province. I, II, III, and IV, respectively, represent the mountainous region of Wuyi Mountain; the coastal low mountain and hill region of Zhejiang and Fujian; the mountainous and hill region in Jiangxi, Fujian, and Guangdong; and the coastal hill and plain region of Fujian and Guangdong. The demarcation line is that between the middle and southern subtropical zones.

2.2. Data and Preprocessing

2.2.1. Phenological Data

The phenological data were obtained from the MCD12Q2 (version 6) land cover dynamics product of the National Aeronautics and Space Administration's (NASA's) Terra and Aqua satellites combined Moderate Resolution Spectroradiometer (<https://lpdaac.usgs.gov/>, accessed on 16 February 2023). It is a yearly dataset with a spatial resolution of 500 m, extending from 2001 to 2019. In this dataset, the vegetation index is the 2-band Enhanced Vegetation Index (EVI), which is calculated from the MODIS Nadir Bidirectional Reflectance Distribution Function–Adjusted Reflectance for the time series. After filling in the missing values contaminated by snow, rain, clouds, and other factors, cubic spline smoothing is used to recreate the EVI time series. The EVI time series interval of continuous growth and fall is judged using the sliding window method. An interval is considered to be in a growth cycle when both its highest value and amplitude are equal to the designated thresholds. The phenological datasets involve the determination of phenological change dates, which are derived from the extreme points of the curvature variations relative to the curve that the logistic function has fitted to the growth cycle [40]. The date of phenology is generally expressed using the day of year (doy). The dataset can identify up to two growth cycles. Some forest types in Fujian Province have bimodal EVI curves. However, because of the tiny variation between the two peaks, the dataset was unable to capture the difference between the two growth seasons. Even if there is only one growing season, the variation between the two peaks can be reflected in the fluctuation of the EOS. To date, the dataset has been used to study phenological changes on a global scale [41–43], and has shown a high correlation with ground observation data in Alberta [44]. For comparison with this data, we utilized the phenological measurement data from Fujian Province in the earlier literature [45]. Although the EOS range came a bit later, it produced a consistent SOS range and consistent spatial distribution findings. The SOS, EOS, LOS, and POP datasets of forest

remote-sensing images from 2001 to 2019, after image preprocessing, were used as the phenological spatial and temporal characteristics and to carry out driving-force analysis.

2.2.2. Thematic Data

The land-cover data were obtained from the European Space Agency's Climate Change Initiative product, and achieved a spatial resolution of 300 m (<https://www.esa-landcover-cci.org/>, accessed on 24 February 2023), the classification scheme of which is based on the United Nations Land Cover Classification System. The product is more accurate and more consistent as to the actual distribution of China's forests than are the other land-cover products [46]. For the classification of forest types, the area of closed to open (>15%) forests is defined as the main forest type of the pixel. Mixed pixels of trees and shrubland, grassland, or other vegetation are also present in the product. Because the forest coverage area in the mixed image is smaller, spectral differences exist in the areas that have greater forest coverage and other vegetation in common, which causes information errors. Thus, the mixed forest pixels were removed in this study. In recent years, China's land cover pattern has changed rapidly. To ensure the spatial consistency of the distribution and forest types, the areas in which product extraction did not change from 2001 to 2019 were selected. The obtained forest types include evergreen needleleaf forests (ENF) and evergreen broadleaf forests (EBF), deciduous broadleaf forests (DBF1), and closed (>40%) deciduous broadleaf forests (DBF2). It also includes vegetation dominated by shrubland (SHL). Since deciduous broadleaf forest makes up a small portion of the forest types in Fujian Province, it is frequently accompanied by other surface vegetation. Among them, "closed (>40%)" means that the pixel includes a certain area of upper, middle, and lower trees and shrubs in addition to the deciduous broadleaf forest. Therefore, the categorization in the source data was maintained, and it separated deciduous broadleaf forest into two groups, namely, closed >15% (DBF1) and closed to open >40% (DBF2). ENF and DBF2 were mainly distributed in region I, EBF was mainly distributed in regions I and III, and DBF1 and SHL were mainly distributed in region IV (Figure 2a). The altitude distribution of most pixels of the five forest types was approximately 500 m. For the most part, DBF2 had the highest altitude distribution, while SHL had the lowest (Figure 2b).

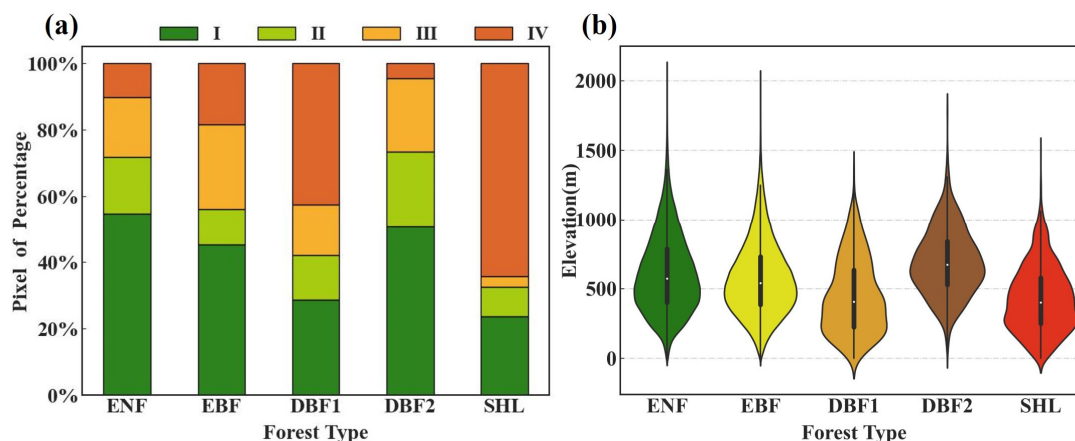


Figure 2. (a) The proportions of individual regions in the area as to distinguished forest types. (b) The elevation distribution of different vegetation types in Fujian Province. In the figure, ENF, EBF, DBF1, DBF2, and SHL, respectively, represent evergreen needleleaf forests, evergreen broadleaf forests, deciduous broadleaf forests, closed (>40%) deciduous broadleaf forests, and shrubland.

The National Earth System Science Data Center, National Science and Technology Infrastructure of China (<http://www.geodata.cn/>, accessed on 21 February 2023) offers gridded monthly temperature and precipitation datasets, spanning from 2000 to 2020, with a spatial resolution of 1 km [47]. These datasets were generated by downscaling in China via the Delta spatial downscaling scheme, based on the global 0.5° climate dataset

released by the Climate Research Unit and the high-resolution climate dataset released by WorldClim. The raster data of the SOS and EOS were combined to locate the beginning and end months of the growth period of each pixel. The raster data of precipitation and temperature, with a lag of 0–3 months and an accumulation of 2–3 months, from 2001 to 2019 were then obtained according to the monthly precipitation and temperature data, which were used to input the independent variables of the climate factors in GeoDetector.

The digital elevation model utilized the Shuttle Radar Topography Mission data of the United States Space Shuttle Endeavour, with a resolution of 90 m (<https://www.earthdata.nasa.gov/>, accessed on 27 February 2023). The slope and aspect data were calculated based on elevation data. To discretize the topographic factors, the elevation, slope, and aspect data were respectively divided into four, six, and nine categories according to the basic landform types of China [48] and the Operational Rules for the Ninth National Forest Resources Inventory in Fujian Province (https://fzly.fuzhou.gov.cn/zwgk/ztl/rcl/zybh/201803/t20180306_2023061.htm (accessed on 8 March 2023)). The results after the division are shown in Figure 3.

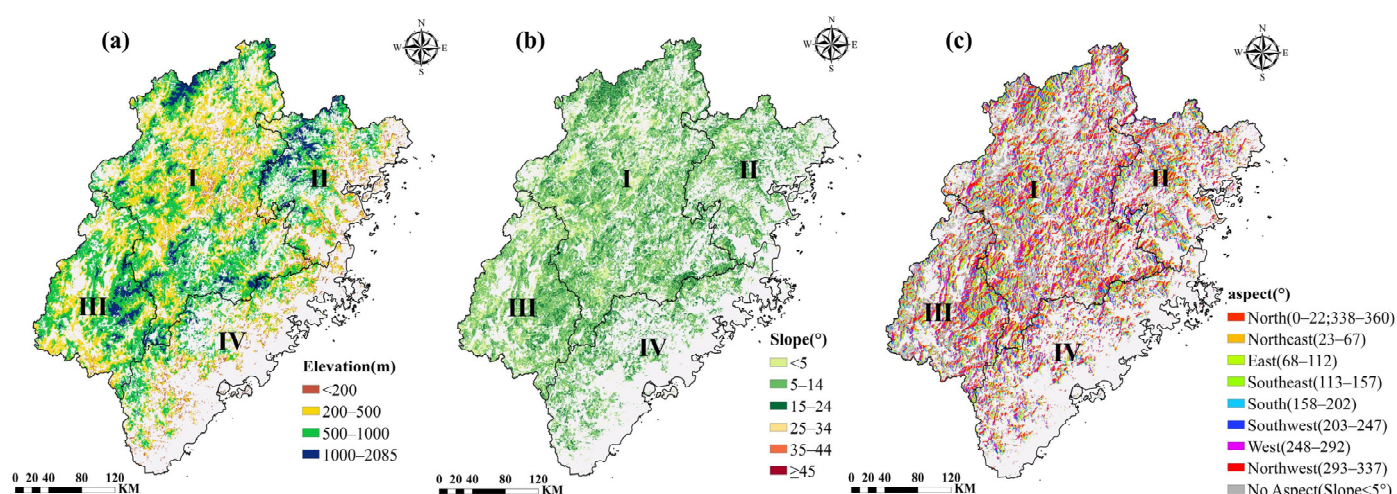


Figure 3. The division of the (a) elevation data, (b) slope data, and (c) aspect data in Fujian Province.

2.3. Methods

2.3.1. Workflow

Based on the datasets, the workflow of this research is shown in Figure 4. To begin, the spatiotemporal variation of phenology was analyzed by calculating the mean values of the SOS, EOS, LOS, and POP phenologies on a pixel-by-pixel basis for each year. Theil–Sen (Sen) median analysis and the Mann–Kendall (MK) test were employed to analyze the change trends at the pixel level, as these tests can derive phenological differences across areas. Then, the raster data of forest phenology were used to locate the beginning and ending months of the growing season pixel by pixel; these were then combined with the monthly precipitation and temperature data to calculate the annual raster data with a lag of 0–3 months and an accumulation of 2–3 months. Finally, the dependent variables were the SOS and EOS. The discrete variables of lagged and cumulative air temperature and precipitation, forest type, and topographic factors were used as independent variables. Regarding GeoDetector, factor, interaction, risk, and ecological detection were utilized to understand the degrees to which individual and combined factors had effects on the SOS and EOS. The key determinants of phenological spatial heterogeneity were identified.

$$S = \sum_{i=1}^{n-1} \sum_{j=i+1}^n \text{sgn}(SOS_j - SOS_i) \tag{3}$$

$$\text{Var}(S) = \frac{n(n-1)(2n+5)}{18} \tag{4}$$

In Equation (3), $(SOS_j - SOS_i)$ is the difference between the SOS values of years j and i , and $\text{sgn}(\theta)$ is a sign function, which is calculated by Equation (5). In Equation (4), n is the length of the time-series, and the value of n in this study is 19.

$$\text{sgn}(x_j - x_i) = \begin{cases} +1, & SOS_j - SOS_i > 0 \\ 0, & SOS_j - SOS_i = 0 \\ -1, & SOS_j - SOS_i < 0 \end{cases} \tag{5}$$

According to the positive and negative values of β , the Sen trend is divided into delayed, advanced, and no fluctuation. When the standardized statistics are $|Z| \geq 1.65$, $|Z| \geq 1.96$, and $|Z| \geq 2.58$ at the 0.01, 0.05, and 0.001 significance levels, respectively, the null hypothesis of no trend is rejected, as shown in Table 1. The spatiotemporal trend of phenology was finally discovered.

Table 1. The significance classification of the phenological trends.

β	Z	Trend Significance Classification
$\beta > 0$	$2.58 < Z$	Extremely significantly delayed
	$1.96 < Z \leq 2.58$	Significantly delayed
	$1.65 < Z \leq 1.96$	Slightly significantly delayed
	$Z \leq 1.65$	Not significantly delayed
$\beta = 0$	Z	No fluctuations
$\beta < 0$	$Z \leq 1.65$	Not significantly advanced
	$1.65 < Z \leq 1.96$	Slightly significantly advanced
	$1.96 < Z \leq 2.58$	Significantly advanced
	$2.58 < Z$	Extremely significantly advanced

Note: β is the median value of the slope of the phenological parameter, and Z is the statistic for the significance test.

2.3.3. GeoDetector

GeoDetector was used to detect the spatial differentiation of the SOS and EOS, reveal the driving force behind the geographical differentiation, and explore the degrees of influence of various factors on the phenological parameters [32]. It has been used in the study of spatial and temporal dynamic driving forces, such as vegetation cover, land aridification, and landscape-pattern changes [51–54]. The principle is to judge the relationships between spatial heterogeneity and potential driver factors through variances. If a driver factor has an important impact on the dependent variable, the spatial distribution of the driver and the dependent variable should be similar. The q -value calculated using variance was used to quantify the degree of single-factor and two-factor driving. The independent variables were discretized during GeoDetector preprocessing; the values of all the independent variables represent the data intervals. The functions of GeoDetector include factor, interaction, risk, and ecological detection.

The SOS/EOS and driving factor X pixel values corresponding to the same position were extracted through gridding. The grid points each represent a spatial range of 500 m × 500 m, which is consistent with the spatial resolution of MCD12Q2. The point-data were fed into the “GD” package [55] in R 4.2.2 [56] to run the GeoDetector model and explore the driving forces behind the spatiotemporal differentiations between the SOS and EOS. Topography, weather, forest type, and time lags were taken into account when choosing the driving factors. Previous research selected 3 months as a threshold for the time-lag response of terrestrial plant development at the world scale or forest growth at the regional scale within Fujian Province [18,28,57,58]. The lagged and cumulative datasets

were created by choosing time windows of 0–3 months for the meteorological parameters and combining them with the phenological months. Table 2 displays the descriptions and value ranges of the factors.

Table 2. The descriptions of the GeoDetector factors.

Factor	Description	Value Range	Unit
X ₀	Forest type	ENF; EBF; DBF1; DBF2; SHL	\
X ₁	Elevation data	[0, 2085]	m
X ₂	Slope data	[0, 50.4]	°
X ₃	Aspect data	[−1.0, 360.0]	°
X ₄	Monthly average precipitation	(175.9, 2711.7]	0.1 mm
X ₅	Monthly average air temperature	(3.2, 22.6]	°C
X ₆	Monthly average precipitation in the previous month	(174.1, 1972.5]	0.1 mm
X ₇	Monthly average temperature in the previous month	(1.6, 24.4]	°C
X ₈	Monthly average precipitation two months ago	(248.8, 2488.7]	0.1 mm
X ₉	Monthly average temperature two months ago	(0.4, 27.0]	°C
X ₁₀	Monthly average precipitation three months ago	(182.8, 3241.7]	0.1 mm
X ₁₁	Monthly average temperature three months ago	(−0.1, 28.4]	°C
X ₁₂	Accumulated average precipitation in the past two months	(266.7, 1789.4]	0.1 mm
X ₁₃	Accumulated average temperature in the past two months	(1.5, 25.7]	°C
X ₁₄	Accumulated average precipitation in the past three months	(308.8, 2083.5]	0.1 mm
X ₁₅	Accumulated average temperature in the past three months	(1.2, 26.4]	°C

Note: The value ranges of variables X₄ and X₁₅ are the common values of the temperature or precipitation datasets derived from the monthly positioning of SOS and EOS data.

Factor detection explores the single-factor effects on the spatial differentiation of the phenological parameters, and the explanatory degree of each factor is measured by the *q*-value, the equations for which are as follows.

$$q = 1 - \frac{\sum_{h=1}^L N_h \sigma_h^2}{N \sigma^2} = 1 - \frac{SSW}{SST}, q \in [0, 1], \tag{6}$$

$$SSW = \sum_{h=1}^L N_h \sigma_h^2, SST = N \sigma^2, \tag{7}$$

where *q* measures the degree to which the terrain and climate factors explain the phenological parameters, *h* is the stratification of variable *Y* or the classification of factor *X*, and *N_h* and *N* are the numbers of spatial units of the *h* classification and the whole area, respectively. Moreover, σ_h^2 and σ^2 are the variances of the *Y* values of the *h* layer and the whole area, respectively, and *SSW* and *SST* are the sum of variance within the layer and the total variance of the whole area, respectively.

Interactive detection mainly evaluates the degree to which the spatial heterogeneity of phenology is explained by combined factors. The *q*(*X*₁ ∩ *X*₂) is formed by stacking the two variables together to calculate the *q*-value of the interaction. A determination is made as to whether the combined influence of the two elements is enhanced, weakened, or independent of one another by comparing the separate *q*-values (*q*(*X*₁), *q*(*X*₂)) and *q*(*X*₁ ∩ *X*₂). The comparison criteria for *q*-values and interaction types are shown in Table 3.

Table 3. The types of interaction between two independent variables.

Interaction Types	Judgement Criteria
Nonlinear weakened	$q(X_1 \cap X_2) < \text{Min}(q(X_1), q(X_2))$
Univariate weakened	$\text{Min}(q(X_1), q(X_2)) < q(X_1 \cap X_2) < \text{Max}(q(X_1), q(X_2))$
Bivariate enhanced	$q(X_1 \cap X_2) > \text{Max}(q(X_1), q(X_2))$
Independent	$q(X_1 \cap X_2) = q(X_1) + q(X_2)$
Nonlinear enhanced	$q(X_1 \cap X_2) > q(X_1) + q(X_2)$

Note: *q* is the number that quantifies the degree of influence of the driving factor.

Risk detection mainly determines whether there is a significant difference in the phenological mean between two factor regions via a t test. The formula is given by Equation (8), where $\bar{Y}_{h=1}$ represents the mean value of the attribute in subregion h , n_h is the number of samples in the subregion, also called the number of pixels, and Var represents variance.

$$t_{\bar{y}_{h=1}-\bar{y}_{h=2}} = \frac{\bar{Y}_{h=1} - \bar{Y}_{h=2}}{\left[\frac{Var(\bar{Y}_{h=1})}{n_{h=1}} + \frac{Var(\bar{Y}_{h=2})}{n_{h=2}} \right]^{1/2}} \quad (8)$$

Ecological detection explores the significant differences in the effects of the interactions of different factors on the spatial distribution. The formula is given by Equation (9), where N_{X_1} and N_{X_2} , respectively, represent the sample sizes of the two factors X_1 and X_2 , and SSW_{X_1} and SSW_{X_2} , respectively, denote the sum of within-layer variances of the stratification formed by X_1 and X_2 . The calculation formula is given by Equation (10), where L_1 and L_2 , respectively, represent the numbers of layers of variables X_1 and X_2 .

$$F = \frac{N_{X_1}(N_{X_2} - 1)SSW_{X_1}}{N_{X_2}(N_{X_1} - 1)SSW_{X_2}} \quad (9)$$

$$SSW_{X_1} = \sum_{h=1}^{L_1} N_h \sigma_h^2, SSW_{X_2} = \sum_{h=1}^{L_2} N_h \sigma_h^2 \quad (10)$$

3. Results

3.1. Spatial Pattern of the Phenological Parameters

Figure 5 depicts the spatial patterns of the phenological parameters and the differences in the phenological mean values among different forest types and elevations. The spatial patterns of the four phenological parameters display characteristics of spatial heterogeneity with different elevations, site areas, and forest types. The overall pattern of the SOS exhibited an advance from northeast to southwest. Specifically, the SOS started earlier at the junction between region I and region III, and also that between region I and region IV, at approximately 73–96 doy. In the north of region I and the west of region II, the SOS began later, at about 90–136 doy (Figure 5a). The EOS presented a spatial feature of gradual advancement from the coast to the inland region (Figure 5b), and most occurred at 324–344 doy. The LOS was affected by the spatial characteristics of the SOS and EOS, so it appeared to have a spatial pattern of shortening in site areas I, II, and III from the boundary to the middle of the site areas, with the average value mostly ranging from 234 to 260 doy. However, overall, the LOS was longer in region IV (Figure 5c), at about 247–296 doy. The POP presented a pattern of advancement from the coast to the inland region (Figure 5d), which was similar to the EOS pattern, and centered on 183–201 doy overall. To explore the spatial patterns of phenology in detail, the phenological parameters and elevation data were used for regression analysis to explore the altitude gradient of phenology. As the elevation increased by 1000 m, the SOS was significantly delayed by 8 d ($p < 0.05$), whereas the EOS and POP were significantly advanced by 11 and 5 d, respectively, and the LOS was significantly shortened by 19 d (Figure A1).

From the perspective of the forest type, the SOS, EOS, and POP of SHL were later than those of the other four forest types (Figure 6a,b,d), and the LOS was longer (Figure 6c). Moreover, the SOS, EOS, and POP of DBF2 were advanced, while the LOS was shorter. The ENF and EBF experienced little fluctuation in different regions, and the regional mean sizes were similar. However, the SOS and POP of DBF1 fluctuated greatly among the site areas (Figure 6a,d); in particular, the difference in the POP between regions I and II was large (Figure 6d).

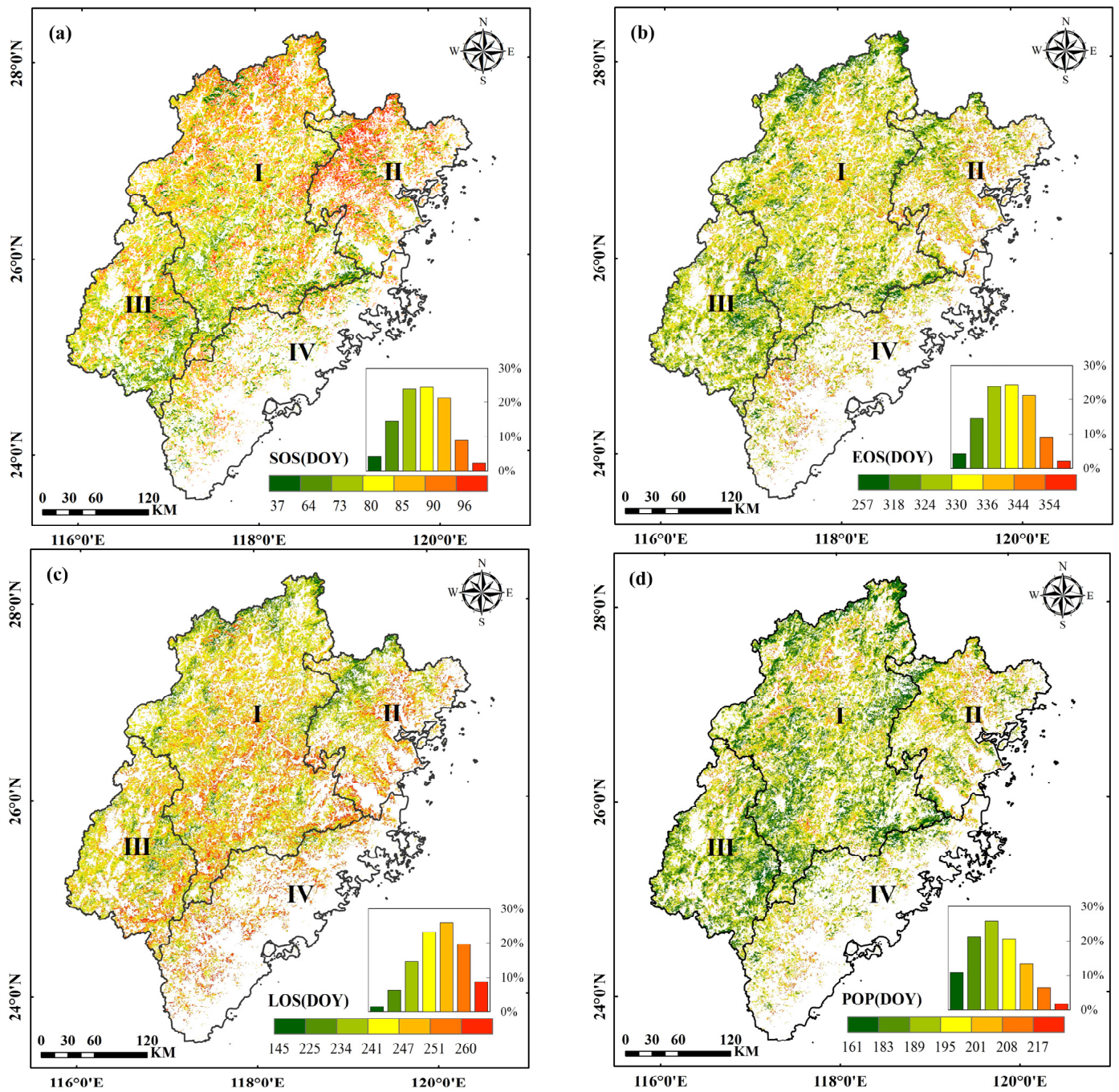


Figure 5. The spatial distributions of the (a) SOS, (b) EOS, (c) LOS, and (d) POP in the Fujian province. The histograms present the proportion of pixels in the phenological interval. DOY indicates the day of the year.

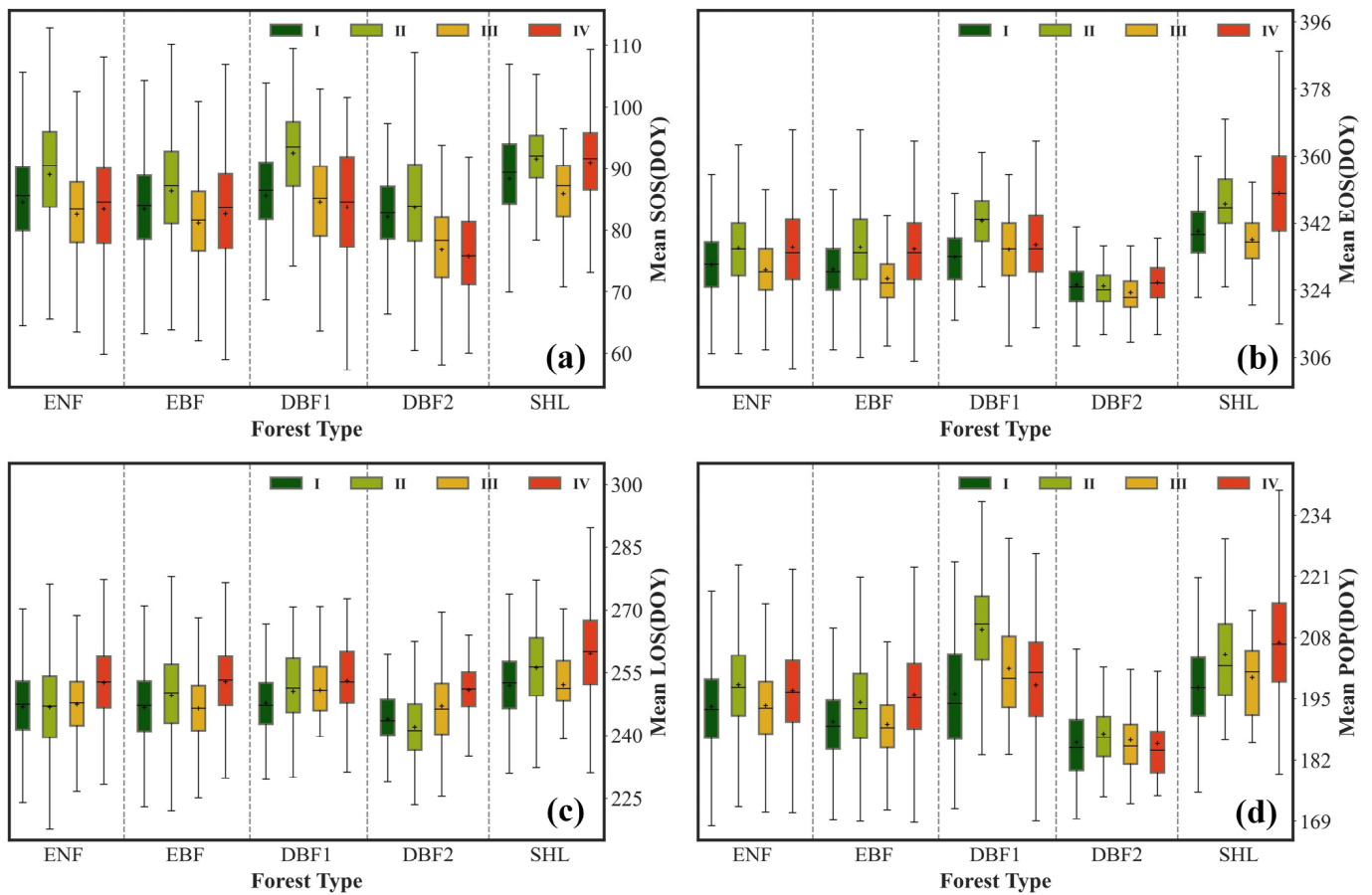


Figure 6. The fluctuations of the (a) SOS, (b) EOS, (c) LOS, and (d) POP among different forest types and site areas.

3.2. Variation Trends of the Phenological Parameters

3.2.1. Temporal Variability of the Mean

As shown in column (f) of Figure 7, the overall forest SOS was, not significantly, advanced at a rate of 0.15 days per year ($p > 0.05$), while the EOS and POP were significantly advanced by 0.51 and 0.57 days per year, respectively. The LOS decreased by 0.36 days per year due to the more advanced trend of the EOS, compared to the SOS, but the trend was not significant ($p > 0.05$). The overall fluctuation range of the SOS was the largest (25 d), followed by the LOS and POP (23 and 22 d, respectively), and finally the EOS (16 d). At the regional scale, the advancement trends presented by the four sites were generally consistent with the overall pixels. Among all the phenological parameters, the fluctuation ranges of the SOS in different regions were relatively coincident, but that of DBF2 in regions III and IV was lower than the others (Figure 7d). Moreover, the overall fluctuation of the four phenological parameters of SHL and DBF1 presented differences; SHL exhibited the largest fluctuation in the EOS (30 d), and the largest fluctuation for DBF1 was in the POP (33 d).

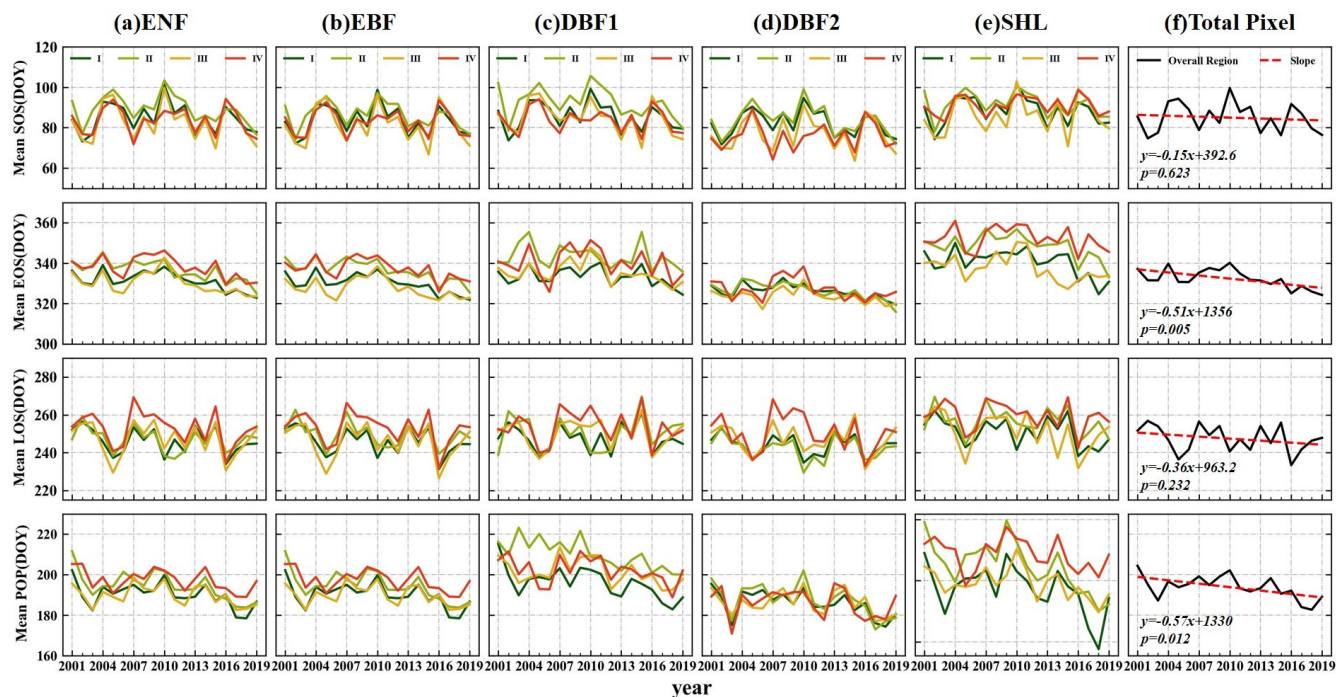


Figure 7. The phenological time trends of (a) evergreen needleleaf forests, (b) evergreen broadleaf forests, (c) deciduous broadleaf forests, (d) deciduous broadleaf forests mixed with other vegetation, and (e) shrubland, in the four site areas, as well as that of (f) all forest pixels.

3.2.2. Variation Trends of the Regions

Figure 8 depicts the geographical distributions of the phenological parameter trends over the past 19 years, as obtained via Sen and MK analysis, as well as the differences in the variation trends of the plot areas and forest types. More than 50% of the pixels for all phenological parameters showed an advanced trend. In terms of SOS and LOS, EOS and POP showed a broader spatial distribution of advance trends (Figure A2a,d,g,j), which account for 74% and 71.3% of the total, respectively. However, most of the advanced trends in these four phenological parameters were not significant. Specifically, the proportions of pixels that showed significant advancement were only 5.6%, 20.5%, 12%, and 17.7% for SOS, EOS, LOS, and POP, respectively, whereas the proportions of pixels that did not show significant advancement were 51.1%, 53.5%, 51.7%, and 53.6%. Furthermore, in comparison to EOS and POP, with 19.2% and 23%, SOS and LOS show a relatively higher proportion of delayed pixels (Figure A2c,f,i,l), accounting for 31.4% and 30.1%, respectively. Nevertheless, the observed trends were predominantly insignificant, with only 1.3%, 2.3%, 1.2%, and 1.5% of the trends being significant for SOS, EOS, LOS, and POP, respectively. Regarding the trend of no fluctuation, SOS and EOS exhibited a relatively larger proportion (Figure A2b,e,h,k), accounting for 11.9% and 6.8% of the total pixels, respectively. Following them were LOS and POP, with proportions of 6.2% and 5.7%, respectively.

Table 4 shows different site-area pixel proportions in the same trend category and the advanced or delayed pixel proportions of different forest types. The areas with a significantly advanced SOS were mainly concentrated in region II, followed by region I. Furthermore, region I had the highest proportion of places with nonsignificant advancement, no fluctuation, and nonsignificant delay, followed by region III. The significantly delayed areas were mainly focused in region I, followed by region IV. In addition, the highest proportion of extremely significant trends was in region IV, followed by region I. The higher values for areas of all trends in the EOS, LOS, and POP were concentrated in region I, as opposed to the those of the SOS advanced trends. Regions III and IV also accounted for large proportions of delayed trends. From the perspective of forest type, the advanced trend was greater than that of the delayed trend in all forest types. DBF1,

ENF, EBF, and DBF2 were the most advanced forest types, corresponding to the SOS, EOS, LOS, and POP, and severally accounting for 72%, 80%, 69%, and 78%, respectively. The proportion of the delayed trend of the EOS in DBF1 accounted for the largest value, at 47%. Regarding the SOS, LOS, and POP, the delayed trends in SHL accounted for the largest proportions, namely, 49%, 39%, and 33%, respectively.

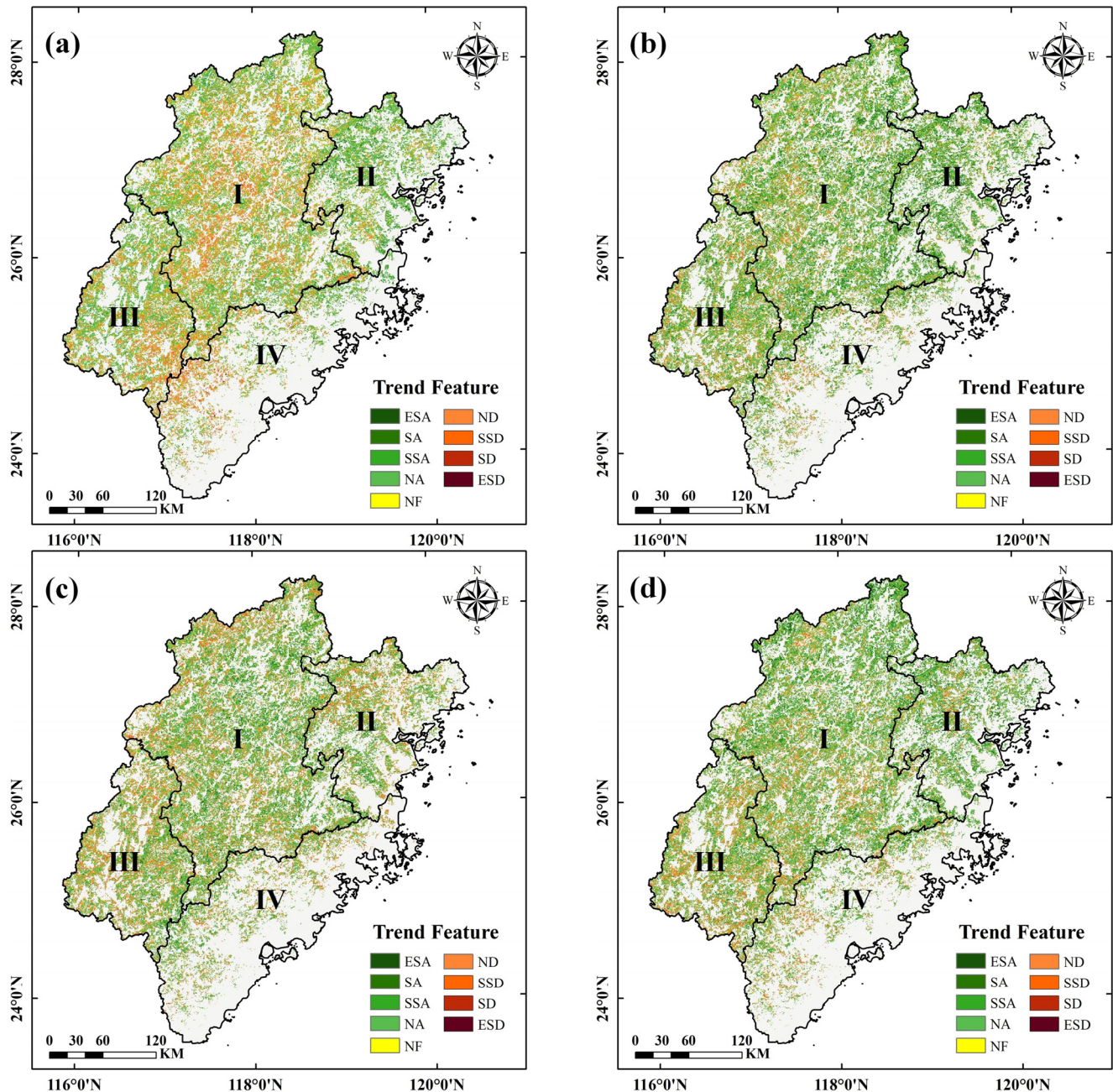


Figure 8. The trend figures of the (a) SOS, (b) EOS, (c) LOS, and (d) POP. In this figure, ESA (ESD), SA (SD), SSA (SSD), NA (ND), and NF, respectively, represent the trends of extremely significantly advanced (or delayed), significantly advanced (or delayed), slightly significantly advanced (or delayed), not significantly advanced (or delayed), and no fluctuation.

Table 4. A pixel-proportions table describing site areas as to the same trend and the advanced or delayed trend proportions in different forest types.

Period	Site Area	ESA	SA	SSA	NA	NF	ND	SSD	SD	ESD	Trend	ENF	EBF	DBF1	DBF2	SHL
SOS	I	28%	31%	36%	51%	59%	58%	54%	47%	32%	Advance	66%	60%	72%	65%	51%
	II	40%	42%	36%	19%	13%	8%	4%	3%	2%						
	III	9%	12%	16%	21%	19%	23%	16%	14%	11%	Delay	34%	40%	28%	35%	49%
	IV	23%	15%	12%	9%	9%	13%	26%	36%	55%						
EOS	I	54%	54%	55%	54%	55%	50%	45%	44%	45%	Advance	80%	78%	66%	76%	61%
	II	26%	23%	20%	16%	12%	10%	8%	7%	5%						
	III	13%	15%	16%	20%	23%	25%	28%	29%	23%	Delay	20%	22%	34%	24%	39%
	IV	7%	8%	9%	11%	10%	15%	19%	20%	29%						
LOS	I	65%	61%	59%	54%	53%	48%	47%	46%	51%	Advance	68%	69%	53%	66%	64%
	II	16%	16%	16%	15%	17%	16%	18%	19%	18%						
	III	11%	14%	15%	20%	21%	24%	23%	22%	20%	Delay	32%	31%	47%	34%	36%
	IV	8%	9%	10%	11%	10%	12%	12%	13%	10%						
POP	I	54%	56%	57%	55%	54%	48%	41%	37%	40%	Advance	77%	72%	74%	78%	67%
	II	28%	23%	20%	16%	13%	11%	9%	8%	8%						
	III	11%	13%	14%	19%	23%	27%	33%	35%	34%	Delay	23%	28%	26%	22%	22%
	IV	7%	8%	9%	10%	11%	14%	16%	19%	17%						

Note: SOS, EOS, LOS, and POP represent the start of the growth season, the end of the growth season, the length of the growth season, and the date-position of peak value, respectively. ESA (ESD), SA (SD), SSA (SSD), NA (ND), and NF, respectively, represent the trends of extremely significantly advanced (or delayed), significantly advanced (or delayed), slightly significantly advanced (or delayed), not significantly advanced (or delayed), and no fluctuation. ENF, EBF, DBF1, DBF2, and SHL, respectively, represent evergreen needleleaf forests, evergreen broadleaf forests, deciduous broadleaf forests, closed (>40%) deciduous broadleaf forests, and shrubland. Designations I, II, III, and IV, respectively, represent the mountainous region of Wuyi Mountain; the coastal low mountain and hill region of Zhejiang and Fujian; the mountainous and hill region in Jiangxi, Fujian, and Guangdong; and the coastal hill and plain region of Fujian and Guangdong.

3.3. Exploration of the Driving Factors of SOS and EOS Spatial Differentiation

3.3.1. Single-Factor Exploration

Before factor detection, all driving factors must be discretized. The terrain factors have actual division rules, and the forest type data are discrete; however, the temperature and precipitation data intervals across factors are diverse, and there are no consistent rules. The “GD” package was used for the automatic identification of the best techniques and classifications for discretization processing. All the data were then divided and the *q*-values for the driving factors were computed for different site areas. Figure 9 shows the degrees of influence of the driving factors that affected the spatial differentiation of the mean SOS and EOS in the four regions in the 19-year observation period. In all regions, the impacts of terrain factors on the SOS were less than those of climate factors. Regions II and III were the most affected by the accumulated precipitation in the previous two months and the precipitation in the previous month (63.7% and 63.9%, respectively). The precipitation in the same month had the highest degree of influence in both regions I and IV (49.9% and 65.2%), but the degree of interpretation was higher in region IV. The temperature in the current month had a higher impact than the other factors in region IV (Figure 9d). In the four regions, the explanatory power of terrain factors as to the EOS was slightly greater than that for the SOS, and the elevation and aspect factors ranked relatively higher. The lagged or cumulative effects of precipitation in the previous two and three months on the EOS ranked in the top four. The types of top-ranked EOS factors were basically the same in the four regions, but the ranking order in region IV was different from those of the others. In summary, precipitation had the highest explanatory power for the SOS and EOS, but the lag time was different. Moreover, terrain factors had more obvious influences on the EOS.

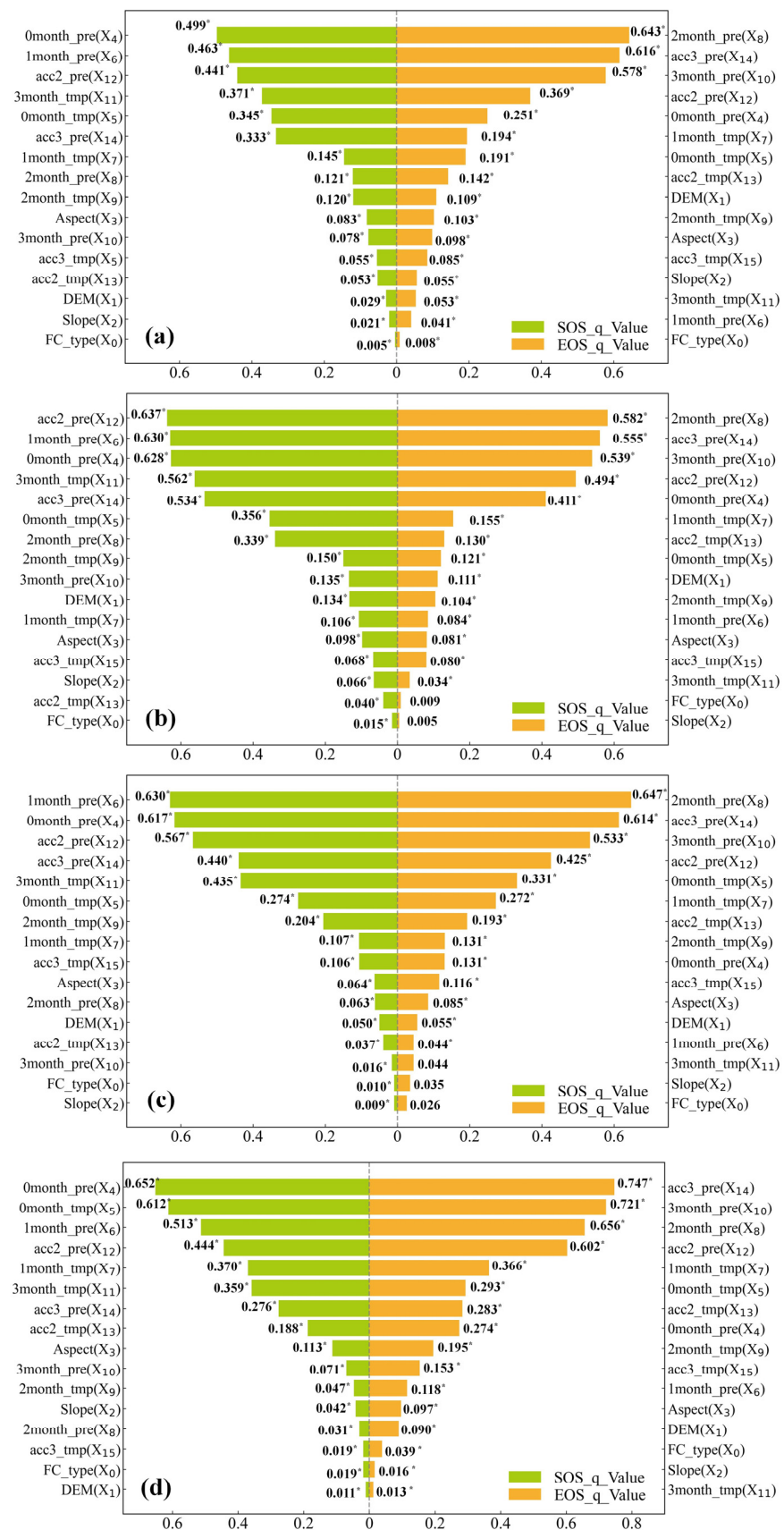


Figure 9. The factor detection q -values of the SOS and EOS in regions (a) I, (b) II, (c) III, and (d) IV. In the figure, “*” means that the factor has passed the significance test. The lagged impacts of precipitation

and temperature are, respectively, presented in the formats “#month_pre” and “#month_tmp,” where “#” represents the number of pre-season months. Moreover, the cumulative impacts are, respectively, presented in the formats “acc#_pre” and “acc#_tmp,” where “#” denotes the cumulative length. Finally, DEM is the elevation, Slope and Aspect are terrain factors, and FC_type is the forest type.

3.3.2. Two-Factor Analysis

According to the factor detection results, the interaction *q*-values between two factors were calculated for different site areas and compared one by one to determine the interaction type and judge whether the two-factor interaction was stronger or weaker than the individual factors. Table 5 lists the top five factor-interactions in the interaction detections of different site areas. In the majority of the factor interactions, the SOS exhibited nonlinear enhancement, and the EOS exhibited bivariate enhancement. This proves that the EOS was not only affected by current factors, but also by other factors, and that the effects of factor interactions on the SOS were stronger. The interaction of the lagged effect of the temperature in the past three months (X_{11}) and the temperature in the current month (X_5) in regions I, II, and III had the strongest explanatory power for the SOS (78.2%, 85.4%, and 76.6%, respectively). In region IV, the interactive effect of X_5 and the precipitation in the current month (X_4) had the strongest explanatory power for the SOS (85.6%). In terms of the EOS, the interaction between the accumulated precipitation in the past three months (X_{14}) and the accumulated temperature in the past two months (X_{13}) had the strongest explanatory power in regions I and IV (83.9% and 85.3%, respectively). The interaction between X_{14} and the lagged effect of the temperature in the previous month (X_7) or in the previous two months (X_9) was the greatest in regions II and III (75.4% and 77.4%, respectively). In general, the interactions between climate factors accounted for the majority. Among the top five factor-interactions, those types involving the SOS in the four regions differed greatly, while those of the EOS were basically the same, but the ranking order demonstrated a difference. The main combined driving factors of the SOS and EOS were any two factors among X_{11} , X_5 , X_4 , X_{14} , and X_7 . The combination of two factors enhanced the interpretation of a single factor. Thus, the factors jointly, not independently, affected the spatial differentiation of phenology.

Table 5. Ranking of *q*-values for interaction exploration.

Period	Site Area	Factor Interaction Ranking
SOS	I	$X_{11} \cap X_5$ (0.782) \uparrow > $X_{15} \cap X_5$ (0.730) \uparrow > $X_9 \cap X_5$ (0.718) \uparrow > $X_6 \cap X_5$ (0.711) $\uparrow\uparrow$ > $X_{12} \cap X_5$ (0.700) $\uparrow\uparrow$
	II	$X_{11} \cap X_5$ (0.854) $\uparrow\uparrow$ > $X_{12} \cap X_5$ (0.849) $\uparrow\uparrow$ > $X_6 \cap X_5$ (0.831) $\uparrow\uparrow$ > $X_{12} \cap X_7$ (0.828) \uparrow > $X_{14} \cap X_5$ (0.819) $\uparrow\uparrow$
	III	$X_{11} \cap X_5$ (0.766) \uparrow > $X_{11} \cap X_4$ (0.739) $\uparrow\uparrow$ > $X_6 \cap X_5$ (0.736) $\uparrow\uparrow$ > $X_5 \cap X_4$ (0.729) $\uparrow\uparrow$ > $X_{15} \cap X_5$ (0.728) \uparrow
	IV	$X_5 \cap X_4$ (0.856) $\uparrow\uparrow$ > $X_7 \cap X_4$ (0.827) $\uparrow\uparrow$ = $X_{12} \cap X_5$ (0.827) $\uparrow\uparrow$ > $X_6 \cap X_5$ (0.816) $\uparrow\uparrow$ > $X_{13} \cap X_4$ (0.811) $\uparrow\uparrow$
EOS	I	$X_{14} \cap X_{13}$ (0.839) \uparrow > $X_{14} \cap X_9$ (0.836) \uparrow > $X_{15} \cap X_{14}$ (0.834) \uparrow > $X_{14} \cap X_7$ (0.827) \uparrow > $X_8 \cap X_7$ (0.804) $\uparrow\uparrow$
	II	$X_{14} \cap X_7$ (0.754) \uparrow > $X_{14} \cap X_{13}$ (0.747) \uparrow > $X_{14} \cap X_9$ (0.735) \uparrow > $X_{14} \cap X_5$ (0.731) \uparrow > $X_8 \cap X_7$ (0.728) $\uparrow\uparrow$
	III	$X_{14} \cap X_9$ (0.774) \uparrow > $X_{15} \cap X_{14}$ (0.770) \uparrow > $X_{14} \cap X_{13}$ (0.767) $\uparrow\uparrow$ > $X_{14} \cap X_7$ (0.763) $\uparrow\uparrow$ > $X_9 \cap X_8$ (0.759) $\uparrow\uparrow$
	IV	$X_{14} \cap X_{13}$ (0.853) $\uparrow\uparrow$ > $X_{14} \cap X_7$ (0.852) $\uparrow\uparrow$ > $X_{14} \cap X_9$ (0.850) $\uparrow\uparrow$ > $X_{15} \cap X_{14}$ (0.845) $\uparrow\uparrow$ > $X_{14} \cap X_{11}$ (0.833) \uparrow

Note: $\uparrow\uparrow$ represents nonlinear enhanced, \uparrow represents bivariate enhanced. This table lists only the top five factor-interactions in terms of *q*-values, with parentheses presenting the *q*-values of the interactions.

3.3.3. Interval Factor Detection

Interval detection is the intermediate result of risk area detection. The driving-factor intervals corresponding to the earliest start/end and the latest start/end of the SOS and EOS were obtained by calculating the phenological mean values in the classification intervals of the discrete driving factors. Then, the specific laws as to the influences of terrain and climate factors on the spatial differentiations of the phenological parameters were obtained. In the period 2001–2019, the SOS and EOS in DBF2 occurred the earliest, and those in SHL occurred the latest (Figure 10a). Regarding elevation, the SOS in the areas with an elevation of less than 200 m occurred the earliest and the EOS occurred the latest, while the opposite was true in the areas with an elevation between 1000 and 2500 m (Figure 10b). These

two conclusions are consistent with the characteristics presented in the spatial distribution patterns of phenology in Section 3.1. Regarding the SOS and EOS, those in the north occurred earlier, while those in the south occurred later (Figure 10c). In terms of the slope, the SOS started earlier and the EOS ended later on gentler slopes, while steeper slopes displayed the opposite trend (Figure 10d).

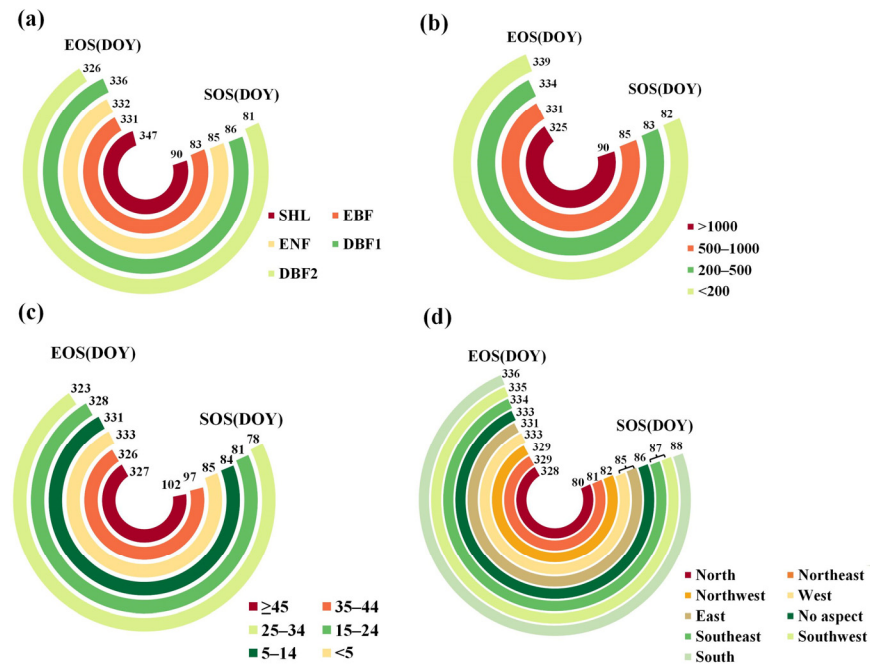


Figure 10. The mean SOS and EOS for (a) forest type, (b) elevation, (c) slope, and (d) aspect factors.

Table 6 reports the intervals corresponding to the maximum SOS and EOS for each lag and accumulation factor. The precipitation factors had a certain positive correlation with the SOS. The SOS had positive relationships with the temperature in the current month, the temperature in the previous month, and the cumulative temperature in the previous two months. Moreover, it had negative relationships with the temperature in the previous two months, the temperature in the previous three months, and the cumulative temperature in the previous three months. The EOS had negative correlations with all precipitation and temperature factors; it occurred earlier in the areas where there was more rainfall and higher temperatures.

Table 6. The earliest or latest intervals and the mean values of the intervals of the SOS and EOS corresponding to the temperature and precipitation factors.

Factor	Range of Max SOS Mean	Max SOS Mean (d)	Range of Min SOS Mean	Min SOS Mean (d)	Range of Max EOS Mean	Max EOS mean (d)	Range of Min EOS Mean	Min EOS Mean (d)
X ₄	(2030, 2710]	95	[456, 896]	67	[176, 288]	343	(991, 1460]	321
X ₅	(17.9, 21.1]	94	[3.2, 8.0]	60	[5.5, 8.9]	344	(17.2, 22.7]	323
X ₆	(1460, 1970]	98	(251, 580]	72	[174, 399]	340	(961, 1430]	329
X ₇	(14.2, 18.3]	92	[1.7, 5.6]	64	[9.1, 12.9]	349	(21.4, 24.5]	323
X ₈	(910, 1480]	89	[266, 557]	80	[249, 635]	344	(1210, 2490]	322
X ₉	[0.4, 5.2]	89	(13.8, 18.7]	71	[13.8, 17.1]	343	(24.8, 27.0]	324
X ₁₀	(681, 749]	86	(965, 1340]	71	[285, 824]	356	(2180, 3240]	324
X ₁₁	[0.1, 6.0]	102	(20.1, 23.6]	75	(24.6, 25.3]	333	(27.7, 28.5]	325
X ₁₂	(1260, 1680]	99	[310, 532]	73	[267, 624]	342	(954, 1790]	322
X ₁₃	(13.4, 18.5]	90	[1.6, 5.6]	72	[11.5, 15.3]	345	(22.9, 25.7]	324
X ₁₄	(939, 1440]	92	[309, 536]	77	[343, 803]	345	(1290, 2080]	324
X ₁₅	(7.1, 8.2]	87	(12.1, 13.3]	80	[13.3, 17.0]	340	(24.2, 26.5]	325

3.3.4. Significance Analysis of Factor Interactions

Ecological detection principally reflects whether there were significant differences in the spatial variation of the SOS and EOS due to each set of driving factors. There were significant differences in the effects of all factors on SOS in regions I and IV. The interactions among the elevation (X_1) and the precipitation in the past three months (X_{10}), the aspect (X_3) and the cumulative temperature in the previous three months (X_{15}), and the monthly precipitation (X_4) and the precipitation in the previous month (X_6) did not have significantly different effects on the SOS in region II. The interactions of the forest type (X_0) and slope (X_2) with X_6 and X_{15} also did not present significant differences (Figure 11a). For the EOS, there were significant differences in the effects between all factors in regions I and II. In contrast, the effects of the interaction between X_4 and the temperature in the previous two months (X_9) in region III, as well as that between X_1 and X_3 in region IV, had no significant difference in the spatial differentiation of the EOS (Figure 11b).

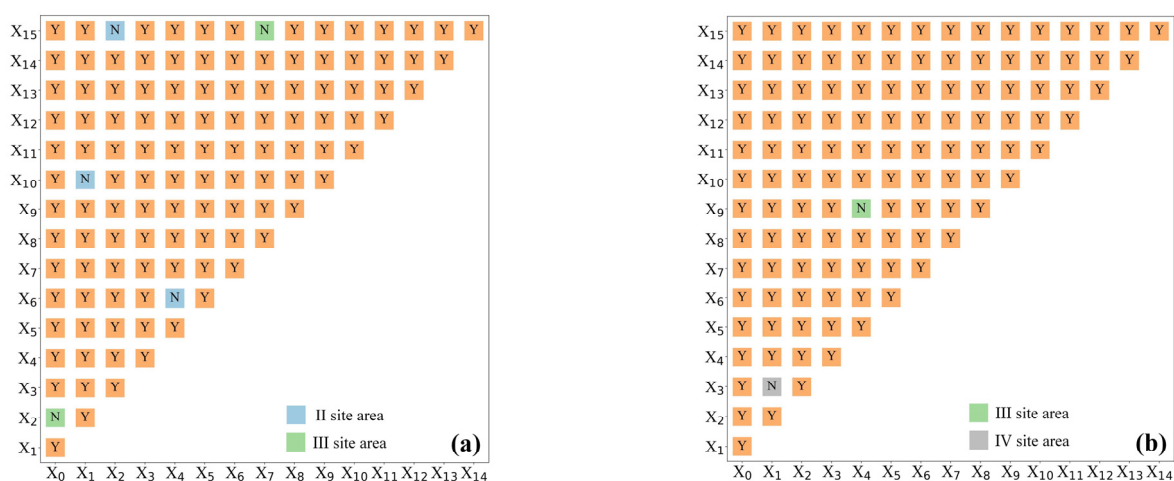


Figure 11. The ecological detection results of the (a) SOS and (b) EOS in site areas. Variables X_0 to X_{15} represent the driving factors, Y indicates that the factor had a significant difference in the 95% confidence interval for the SOS or EOS, and N represents “no significant difference.” The factors with no significant difference were labeled according to different regions, and all the other factors except the labeled ones had significant differences.

4. Discussion

4.1. Spatiotemporal Variation Characteristics of Forest Phenological Parameters

The four phenological parameters of subtropical forests in Fujian showed different spatial patterns; the SOS occurred later in the north and earlier in the south, and the EOS and POP occurred later in the east and earlier in the west, which is similar to the results of previous studies [18,59,60]. Compared with the phenological length in subtropical Mexico, which is in the same latitude zone, the mean values of the EOS and POP were similar, but the SOS was in Fujian later [61], which may be related to the higher mountain altitudes in subtropical Mexico compared to Fujian. However, it is worth noting that the LOS and EOS showed visibly shorter or later phenomena at the junction of the four site regions, as compared with other areas. On the one hand, the junction has a higher elevation (Figure 3a), which indicates that the LOS and EOS are highly sensitive to altitude. On the other hand, the junction is also at the intersection of different growth environments, and the fluctuation of the soil environment and microclimate makes the forest growth unstable. Moreover, the regional growth period within the north and south areas is longer; this is basically consistent with the distribution of tree growth centers, such as Shunchang County and Jiangle County, indicating that the length of the growth period is closely related to forest productivity. In the analysis of phenological mean distributions, there were differences in the central tendencies of different sites and forest types. In most forest types, the concentrated distribution days

of SOS, EOS, and POP in area II were later than other site areas, and the LOS was longer. The central distribution of II and IV was different in most forest types. These regions are located in coastal areas, but also in different subtropical areas. This means that the change in secondary zones could affect the differentiations in phenology. Moreover, the mean phenological distribution of SHL and DBF2 was different from those of other forest types in the same site area. The SOS, EOS, LOS, and POP of SHL distribution were later or longer. Shrublands may extend their growing season to survive, because they have low heat and cold requirements [62]. In contrast to other forest types, DBF2 mixed with more other types of vegetation and showed earlier distribution of SOS, EOS, and POP as well as shorter LOS, suggesting that the increased presence of other vegetation restrained the growth of the forest as a whole. Productivity can be increased through the timely removal of understory vegetation, acceptable levels of thinning to increase the light gap, and the reduction of competition amongst understory plants. The clear geographical difference also offered a relatively high degree of explanation for the driving forces in the GeoDetector model.

From the perspective of the overall time change characteristics, both the SOS and EOS had advanced trends; however, the EOS was noticeably more advanced, causing the LOS to exhibit a shortening trend and the POP to exhibit an advancing trend. The spatial differentiation of the SOS trend was relatively obvious, and most of the delayed trends of the SOS appeared around major rivers. The reason for this could be that the intense disturbances near the river impact the physiological and structural makeup of the forest, and major weather disasters occur when they are severely impacted, which is in line with what is observed in coastal areas. Furthermore, we discovered that the delayed trend was higher in region IV, with the advanced and delayed trends having similar proportions in SHL in SOS and DBF1 in LOS, respectively. This shows that ENF and EBF are more stable than SHL and DBF1. In conclusion, the following measures should be considered for actual production and operation. Mixed forests should be planted at the intersection of forest sites to increase the stability of the forest, and growing trees next to rivers requires careful consideration of a variety of issues. On the one hand, tree species' resistance to waterlogging must be taken into account; on the other hand, to keep rivers flowing, the area of forests must be considered. Evergreen arbor species may be preferable for urban forest greening, as SHL and DBF have weak stability, and SHLs do not have good environmental adaptability in humid and coastal subtropical climates.

4.2. Exploration of the Drivers of the SOS and EOS

According to the study on the influences of the driving factors via GeoDetector, the top five factors affecting the spatial differentiation of the SOS and EOS in the four regions were the same, and these parameters were primarily affected by the lagged effect of pre-season precipitation. This suggests that rainfall is the primary driver, a phenomenon resembling tropical and subtropical forest phenology in North and South America [63]. However, the lag lengths of the dominant factors of the SOS and EOS were different. The main influencing factors of the SOS in regions I, III, and IV were the lag factors of the precipitation in the current and previous months, respectively, and that in region II was the cumulative precipitation in the previous two months. These findings indicate that the production of new forest leaves in region II may require a higher water content. Precipitation is a main influencing factor in most places because it occurs before the growing season, and proper precipitation can encourage spring leaf growth. For the EOS, the precipitation from two months prior was the main driving factor of the regional differentiation in regions I, II, and III, whereas that in region IV was the cumulative precipitation in the past three months. The EOS was also mainly affected by the pre-season precipitation. It is worth noting that the primary EOS factors varied with the difference between the middle and South Asian tropics, and changes in the EOS may also be impacted by variations in soil types.

Despite precipitation having a higher ranking in the SOS single-factor detection, the interaction between the temperature in the first three months of the season and that for the current month had the highest explanatory power for the SOS in regions I, II, and

III, while the interaction between the temperature and precipitation in the current month had the highest explanatory power for the SOS in region IV. The results indicate that the SOS response to temperature is a multi-level response mode, rather than a single-level mode. Moreover, there are also differences between the central tropics and the South Asian tropics. The winter temperature impacts the cooling demands throughout the dormant phase, while the spring temperature is related to the rate of leaf cell division during the growth period. Thus, the spring phenology of the forest is influenced by both the winter and spring temperatures in the subtropical region. In the south subtropics (region IV), the climatic conditions of higher temperature and less precipitation may reduce the heat accumulation demand and increase the demand for precipitation in the bud-recovery stage of the dormant period, resulting in the highest values for interaction between precipitation and temperature for the current month relative to SOS. The explanatory power of the interaction between cumulative precipitation and temperature in the first two months was the highest in regions I and IV, and that of the interaction between cumulative precipitation and lagged temperature was the highest in the other two regions; this is similar to the conclusion of Ren et al. [64]. It was also found that hydrothermal action was more important, and that, although there was no spatial difference between coastal and inland areas, their lags and cumulative lengths were different. Furthermore, the majority of the EOS factor-interactions were bivariate enhanced, indicating that EOS can be influenced by other latent factors in addition to temperature, precipitation, topographical characteristics, and the forest type.

Interval detection can reveal the relationships between phenology and various factors, and the relationships between phenology and the forest type, geography, and climate in Fujian Province were explored in this study. The relationships were found to be basically the same as those in the results of previous analyses of forest types, standing areas, and elevation data, thus demonstrating the reliability of the GeoDetector results. The detection showed that the temperatures at different periods had varied legacy impacts on the SOS (Figure 12a), with a shorter lag and accumulation having a positive effect and a longer lag and accumulation having a negative effect. This also suggests that the requirement for heat varies during the dormant period before leaf growth. Furthermore, temperature and precipitation were both negatively correlated with the EOS (Figure 12b), and the relation between SOS and precipitation was entirely positively correlated. The results for precipitation with SOS and EOS are in line with the findings of Ge et al. [65], who investigated the impact of drought on phenological patterns using the standardized precipitation evapotranspiration index.

In summary, the dominant factors and the degrees of influence showed spatial heterogeneity, and the phenological differentiation in coastal areas II and IV was obvious. Therefore, in actual production, it is necessary to carry out suitable planting and reasonable management activities. The maximum and minimum values in the four site areas were also calculated as a reference for the comparison of recommendations, as shown in Table 7. In region II, thinning should be carried out two months before the start of the growing season (December of the previous year to February) and two months before the growing season ends (August to October). On the one hand, this will change the understory microclimate and reduce the understory species abundance through the gaps in large canopies [66]; on the other hand, more light radiation will penetrate the gaps, which will reduce the soil saturation due to precipitation, thus advancing the SOS, extending the EOS, and lengthening the forest growth period to improve forest productivity. The main focus in region IV should be on the variation of soil moisture throughout the region. Because soil and water loss are more severe when red soil experiences extreme weather, it is vital to limit the planting scale of pure forest and pure shrub areas, and to increase biomass via a combination of irrigation and cash crops. In addition, the growth periods of evergreen trees are longer than those of deciduous trees, so local dominant trees such as *Cunninghamia lanceolata*, *Pinus massoniana*, and *Cinnamomum porrectum* should be planted to the greatest possible extent during afforestation. Simultaneously, in the inland areas with small phenological fluctuations in

regions I and III, attention should be paid to forest tending and management aspects closely related to tree growth, such as release cutting, pruning, and thinning according to forest ages, as well as replanting in areas with low forest density in broadleaf forests.

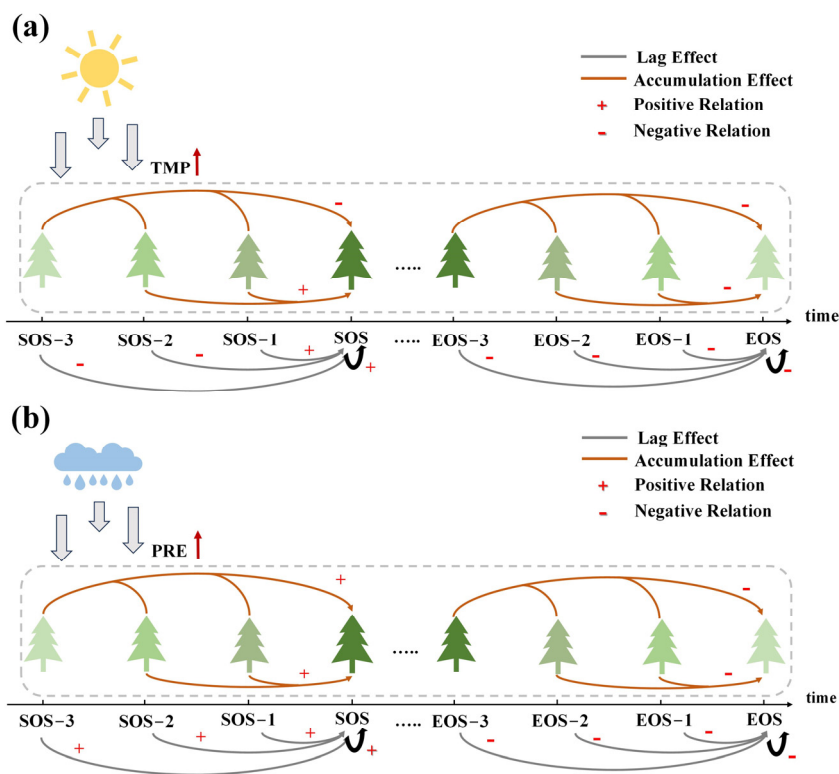


Figure 12. The results of the relationships of lagged and accumulated (a) temperature and (b) precipitation with phenology. TMP indicates temperature and PRE represents precipitation.

Table 7. The operational measures in various regions.

Phenological Parameter	Enhanced Productivity (Prolonged LOS)	Site Area	Reference Value (DOY)	Management Measures
SOS	Advanced (SOS will be advanced by lower temperatures in early spring, higher temperatures in late winter, and less precipitation)	I, III (inland)	73–95 (I) 75–91 (III)	Pay attention to frost disasters, and plant mixed forests near rivers; Selective cutting and interplanting of artificial pure forest.
		II, IV (coastal)	81–100 (II) 79–92 (IV)	Thinning and pruning in late winter and early spring; Choosing evergreen trees.
EOS	Delayed (EOS will be delayed by lower temperatures and less precipitation in summer and autumn)	I, III (inland)	317–344 (I) 319–337 (III)	In the process of tree growth, the forest tending should be strengthened, and the areas with a low density of broadleaf forest should be replanted.
		II, IV (coastal)	324–342 (II) 324–339 (IV)	Reasonable thinning and pruning in summer and autumn; Prevention of extreme weather and planting more local dominant tree species; The planting scale of pure forest and pure shrub areas should be limited, and the mixed planting of arbors and irrigation should be carried out.

Note: The reference value is the number of days in which the main phenological mean interval is centrally distributed.

4.3. Effects of Factor-Driven Tree Physiological Processes on the SOS and EOS

Subtropical forests adapt to changes in climate factors such as light, precipitation, and air humidity through leaf decay. Preseason precipitation was found to have the greatest single influence on the SOS. Trees lose old leaves and develop new leaves when there is no water stress, i.e., when internal and external water values are balanced [67,68]. As a result, before the formation of new leaves, precipitation increases the internal wetness of the tree, allowing it to maximize photosynthesis. However, as the soil moisture approaches saturation, the increase in precipitation contributes to the high water-potential of the trees, which prevents the plants from starting to spread their leaves. However, precipitation is usually accompanied by changes in the soil and surrounding temperature which affect soil respiration and, indirectly, the heat demand for plant growth in spring [69]. The explanatory power of the interaction of preseason temperature was greater than that for precipitation alone. After experiencing low temperatures in autumn and winter, evergreen trees also restrict the growth of bud cells and enter a paradormancy period; the organ enters the endodormancy phase after cold acclimation and enters the ecodormancy phase when cold temperature accumulation reaches a particular level; with the long-term increase in spring temperatures, ecodormancy is disrupted after reaching a specific cumulative temperature, and germination commences [24,26,70,71]. In general, if the temperature rises during the endodormancy period, it will take longer to meet the low temperature requirement, slowing the opening of the ecodormancy phase and delaying bud germination. But, via GeoDetector interval detection, the autumn and winter temperatures (with a long delay) were found to display an opposite relationship. Warming near the endodormancy peak can diminish the depth of bud dormancy, shortening the duration of spring germination and therefore advancing SOS [72]. A warm spring promotes photosynthesis during the spring to advance the SOS, and rising temperatures will reduce the accumulated temperature time and frost damage, advance the leaf emergence time, and have positive effects on trees. High temperatures also increase transpiration and reduce the water intake of trees. In subtropical regions, the negative effects of high temperatures can dilute the positive effects, resulting in the delay of the SOS [73]. Thus, the SOS showed different correlations with temperatures with variations in lag time. During the growth cycle of subtropical forests, the chlorophyll content of leaves decreases as the dry and wet seasons continue [74], and leaf litter usually occurs once or twice. In the second rainy season, the leaves usually tend to balance water loss through stomatal regulation [75]. With open stomata on plant leaves, high temperatures promote photosynthesis and transpiration. In addition, the precipitation makes the soil moist enough. But because of the high temperature, subtropical forests have a large vapor-pressure deficit, which exacerbates tree defoliation and advances the EOS. Therefore, the relationship between temperature, precipitation, and the EOS is negative.

In addition to weather considerations, topographical factors were found to influence the regional differences in the SOS and EOS more than did variation in forest type. However, among the environmental factors, altitude provides a higher degree of explanatory power, and the temperature decreases as the altitude increases (Figure A3a). Reduced ambient temperature inhibits vegetative growth and extends the time it takes for vegetation to achieve the cumulative temperature needed for growth. The terrain of Fujian Province is largely mountainous and hilly, with a distinct microclimate in the mountains and regional precipitation. At low altitudes, the average annual precipitation interval is not greatly altered with elevation (Figure A3c,d), whereas at high altitudes, the average annual precipitation interval increases with elevation (Figure A3e,f). The phenological differentiation caused by precipitation differences was more obvious in high-altitude areas. The link between altitude, temperature, and precipitation caused phenological variations that were consistent with the GeoDetector results. The connection between phenology and elevation, on the other hand, is not a single reaction to temperature or precipitation, and different vertical gradients of phenology will yield distinct driving mechanisms [35,76]. The process behind the vertical properties of phenology is complex; it is controlled by the interplay of evapotranspiration and vegetation, in addition to temperature and precipitation. A unique

phenology is created by a mix of biological and abiotic elements, and the relationships between these factors and phenology must be researched more intensely in the future by collecting more phenological observation data and carrying out experiments.

4.4. Limitations and Uncertainties

The focus of this study was on the effects of lagged climate factors relative to phenological differentiation, and the inclusion of more potential factors like solar radiation, evapotranspiration, a standardized precipitation index, and a standardized precipitation evapotranspiration index in future work may further knowledge of the extent of drought's effects on phenology and reduce the uncertainty of these phenological effects. The spatial resolution of the phenology and land-cover datasets used in this study was relatively low, and some spatial details may have been overlooked that could have affected the results, due to the mountainous and hilly terrain and high vegetation coverage. Fujian Province is prone to tropical cyclones because of its location on the southeast coast, near the western Pacific Ocean. Forest phenology is impacted by subtropical cold waves, freezing rain, and snowfall catastrophes. For example, in addition to a January cold wave in 2016, the summer of that year saw the biggest typhoon since 1949, due to the effects of El Niño, one which severely devastated the vegetation and resulted in the shortest LOS. There are uncertainties in the detection of the EOS, and extreme weather also impacted the original EVI phenological extraction calculation. Chlorophyll and solar-induced chlorophyll fluorescence imagery extracts phenology of subtropical evergreen forests effectively, but the determination of how to assure their spatial resolution at a regional scale to extract phenology remains a challenge. Additionally, experimental research in physiological ecology is important for a thorough understanding of the physiological processes of forest growth and can enhance the comprehension of the underlying mechanisms. Despite these deficiencies, this study revealed the lagged and cumulative effects of temperature and precipitation on forest phenology from a spatial perspective using GeoDetector, analyzed the possible causes of phenological changes, and provided a scientific basis for forest management decisions in Fujian Province.

5. Conclusions

This study analyzed the spatiotemporal characteristics and trends of subtropical forest phenology in Fujian Province from 2001 to 2019 and explored the driving forces of phenological spatial heterogeneity. The findings can provide a reference for phenological research in subtropical regions around the world. The results revealed the following. (1) Spatiotemporal changes and trends were ascertained. The SOS, EOS, LOS, and POP trends were advanced, and the mean values of these were roughly 73–96 day, 324–344 day, 234–260 day, and 183–201 day, respectively. In spatial distribution, the boundaries of site areas had obvious differences on the SOS, EOS, and LOS. From the perspective of forest types, shrubland was found to fluctuate widely, grow late, and have poor stability. (2) Driver factors of phenological differentiation were identified. Precipitation was found to be the dominant individual factor driving the SOS and EOS. But the pre-season intervals varied by locale. In region IV, the interpretation of the SOS and EOS given the precipitation in the current month and the cumulative precipitation in the past three months was the highest among all regions, with values of 65.2% and 74.7%, respectively. The interaction-detection results showed that the SOS was mostly affected by monthly temperature and precipitation in region IV, whereas the interaction effects of monthly present, and for the past three months, temperature were the most important factors impacting the other three regions. The hydrothermal interaction between the precipitation of the past three months and the temperature of the past 1–2 months had the most impact on the EOS. Furthermore, most of the EOSs were bivariate enhanced and impacted by other factors. The relationship between the SOS and temperature was related to the length of time from the interval detection, given that temperature is closely related to bud dormancy. Both temperature and precipitation exhibited negative relationships with the EOS. However,

due to the influence of extreme weather, the detection results for the autumn phenology had limitations. In summary, it is necessary to pay attention to the precipitation in forests in winter and early spring, as well as the effects of extreme natural disasters during the growth period in actual production. In the subsequent phase of analyzing the relationship between phenology and climate, it is suggested that one should consider and quantify the influence of multiple extreme weather factors on tree growth. It is advisable to plant more mixed forests near rivers and the junctions of the site areas and coastal areas to improve the adaptability of forests in the context of climate change. This study explained the driving relationship between subtropical forest phenology and lagged temperature, precipitation and topographic factors, and combined the analysis with actual production principles to guide forestry management to improve forest quality and increase carbon storage. The results are helpful in providing a further scientific basis for further research on subtropical phenology and forest productivity given the backdrop of global warming.

Author Contributions: Conceptualization, M.M. and X.S.; methodology, M.M. and X.S.; software, J.Q., Y.L. and H.Z.; formal analysis, M.M.; resources, M.M. and J.Q.; data curation, H.Z. and Y.L.; writing—original draft preparation, M.M.; writing—review and editing, M.M., B.W., and X.S.; visualization, M.M., J.Q., H.Z. and X.S. All authors have read and agreed to the published version of the manuscript.

Funding: This research was funded by the National Natural Science Foundation of China (Grant number 32101516) and the National Key Research and Development Program of China (Grant number 2023YFD220170401).

Data Availability Statement: Publicly available datasets were analyzed in this study. The data can be found at the following sites: <https://www.esa-landcover-cci.org/> (accessed on 24 February 2023), <https://lpdaac.usgs.gov/> (accessed on 16 February 2023), and <https://www.earthdata.nasa.gov/> (accessed on 27 February 2023). Restrictions apply to the availability of temperature and precipitation data. Data was obtained from National Science & Technology Infrastructure of China and are available at <http://www.geodata.cn/> (accessed on 21 February 2023) with the permission of National Science & Technology Infrastructure of China.

Acknowledgments: Acknowledgement is made for the data support from the National Earth System Science Data Center, National Science & Technology Infrastructure of China (<http://www.geodata.cn>) and the National Aeronautics and Space Administration. We thank NASA for providing free access to their data. We also acknowledge the journal editor and the anonymous reviewers for their insightful criticisms and outstanding work on this research.

Conflicts of Interest: The authors declare no conflicts of interest.

Appendix A

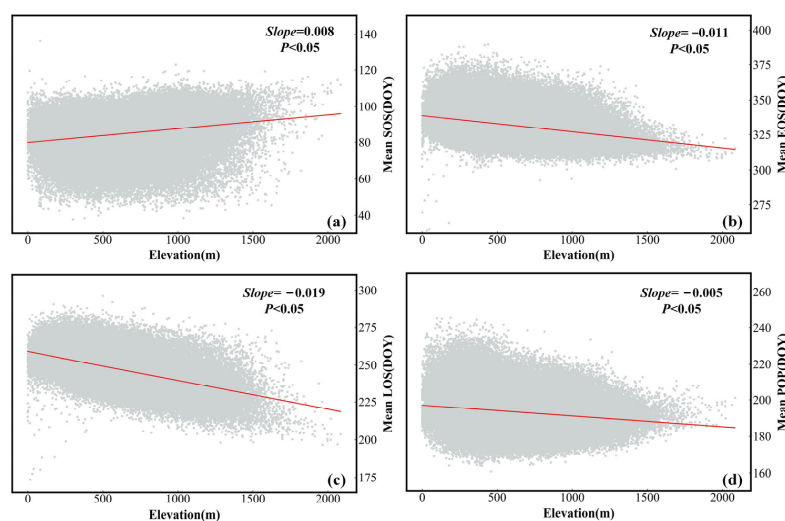


Figure A1. The relationships between altitude and the average (a) SOS, (b) EOS, (c) LOS, and (d) POP.

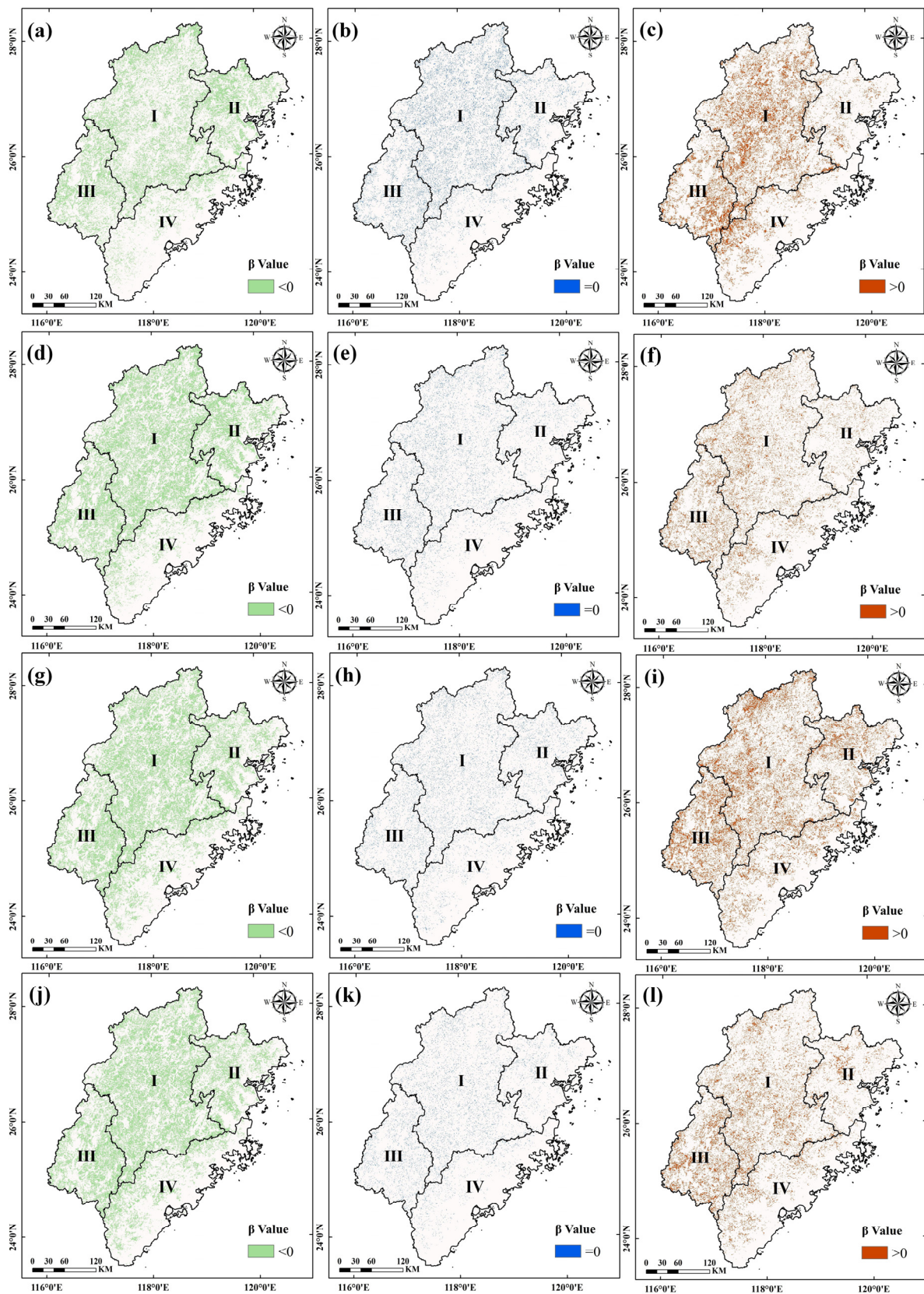


Figure A2. β values of each phenological parameter in the trend analysis. The horizontal axis is arranged from top to bottom to represent the β values of SOS (a–c), EOS (d–f), LOS (g–i), and POP (j–l), respectively. The vertical axis, from left to right, represents the spatial distribution of the β values as follows: less than 0 (a,d,g,j), equal to 0 (b,e,h,k), and greater than 0 (c,f,i,l).

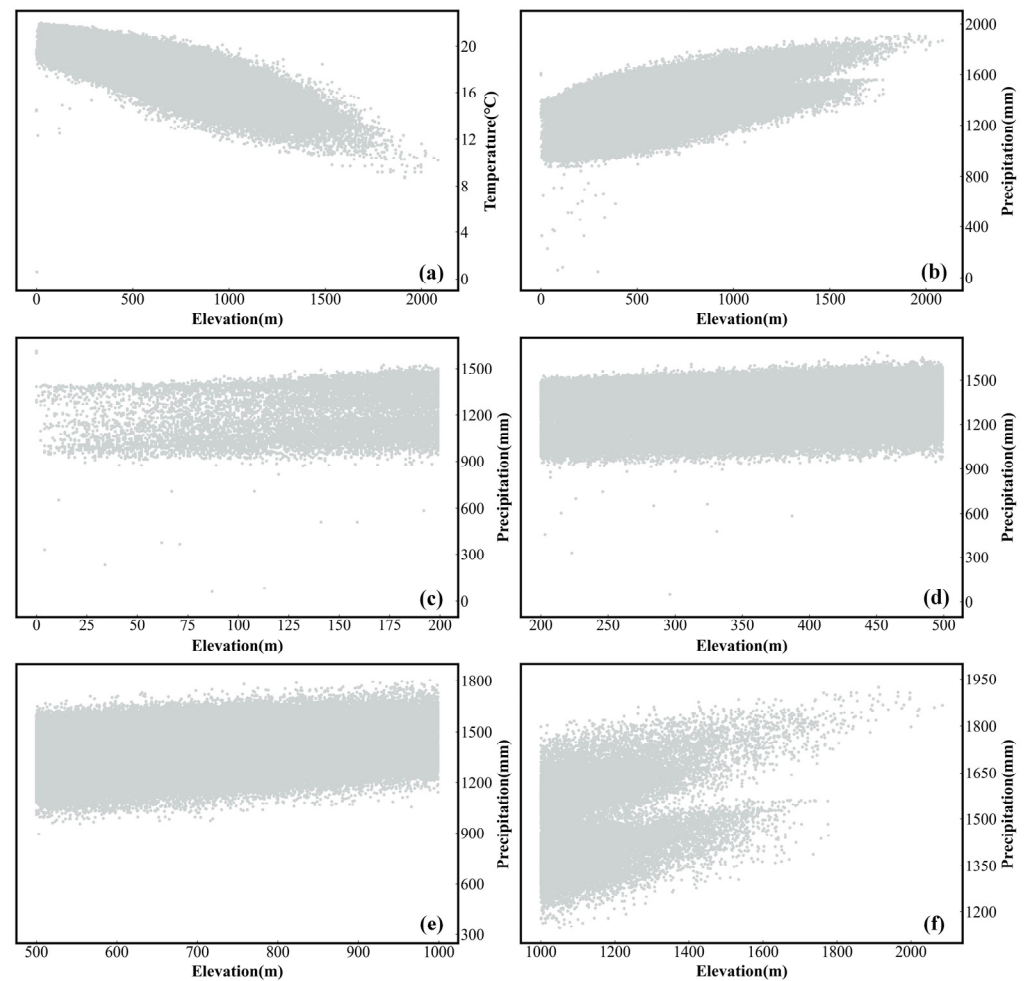


Figure A3. The relationships between altitude and the (a) average annual temperature and (b) precipitation. Subfigures (c–f) show the relationship between elevation and precipitation in different elevation gradients.

References

1. Chmielewski, F.-M.; Rötzer, T. Response of Tree Phenology to Climate Change across Europe. *Agric. For. Meteorol.* **2001**, *108*, 101–112. [[CrossRef](#)]
2. Tan, J.; Piao, S.; Chen, A.; Zeng, Z.; Ciais, P.; Janssens, I.A.; Mao, J.; Myneni, R.B.; Peng, S.; Peñuelas, J.; et al. Seasonally Different Response of Photosynthetic Activity to Daytime and Night-Time Warming in the Northern Hemisphere. *Glob. Chang. Biol.* **2015**, *21*, 377–387. [[CrossRef](#)] [[PubMed](#)]
3. Xia, H.; Qin, Y.; Feng, G.; Meng, Q.; Cui, Y.; Song, H.; Ouyang, Y.; Liu, G. Forest Phenology Dynamics to Climate Change and Topography in a Geographic and Climate Transition Zone: The Qinling Mountains in Central China. *Forests* **2019**, *10*, 1007. [[CrossRef](#)]
4. Savitzky, A.; Golay, M.J.E. Smoothing and Differentiation of Data by Simplified Least Squares Procedures. *Anal. Chem.* **1964**, *36*, 1627–1639. [[CrossRef](#)]
5. Jonsson, P.; Eklundh, L. Seasonality Extraction by Function Fitting to Time-Series of Satellite Sensor Data. *IEEE Trans. Geosci. Remote Sens.* **2002**, *40*, 1824–1832. [[CrossRef](#)]
6. Beck, P.S.A.; Atzberger, C.; Høgda, K.A.; Johansen, B.; Skidmore, A.K. Improved Monitoring of Vegetation Dynamics at Very High Latitudes: A New Method Using MODIS NDVI. *Remote Sens. Environ.* **2006**, *100*, 321–334. [[CrossRef](#)]
7. Klisch, A.; Atzberger, C. Evaluating Phenological Metrics Derived from the MODIS Time Series over the European Continent. *Photogramm. Fernerkund. Geoinf.* **2014**, *5*, 409–421. [[CrossRef](#)] [[PubMed](#)]
8. White, M.A.; Thornton, P.E.; Running, S.W. A Continental Phenology Model for Monitoring Vegetation Responses to Interannual Climatic Variability. *Glob. Biogeochem. Cycles* **1997**, *11*, 217–234. [[CrossRef](#)]
9. Reed, B.C.; Brown, J.F.; VanderZee, D.; Loveland, T.R.; Merchant, J.W.; Ohlen, D.O. Measuring Phenological Variability from Satellite Imagery. *J. Veg. Sci.* **1994**, *5*, 703–714. [[CrossRef](#)]

10. Li, C.; Zhuang, D.; He, J.; Wen, K. Spatiotemporal Variations in Remote Sensing Phenology of Vegetation and Its Responses to Temperature Change of Boreal Forest in Tundra-Taiga Transitional Zone in the Eastern Siberia. *J. Geogr. Sci.* **2023**, *33*, 464–482. [[CrossRef](#)]
11. Li, J.; Guan, J.; Han, W.; Tian, R.; Lu, B.; Yu, D.; Zheng, J. Important Role of Precipitation in Controlling a More Uniform Spring Phenology in the Qinba Mountains, China. *Front. Plant Sci.* **2023**, *14*, 1074405. [[CrossRef](#)] [[PubMed](#)]
12. Yuan, M.; Zhao, L.; Lin, A.; Wang, L.; Li, Q.; She, D.; Qu, S. Impacts of Preseason Drought on Vegetation Spring Phenology across the Northeast China Transect. *Sci. Total Environ.* **2020**, *738*, 140297. [[CrossRef](#)] [[PubMed](#)]
13. Zhou, X.; Geng, X.; Yin, G.; Hänninen, H.; Hao, F.; Zhang, X.; Fu, Y.H. Legacy Effect of Spring Phenology on Vegetation Growth in Temperate China. *Agric. For. Meteorol.* **2020**, *281*, 107845. [[CrossRef](#)]
14. Zhu, W.; Zhang, X.; Zhang, J.; Zhu, L. A Comprehensive Analysis of Phenological Changes in Forest Vegetation of the Funiu Mountains, China. *J. Geogr. Sci.* **2019**, *29*, 131–145. [[CrossRef](#)]
15. Piao, S.; Fang, J.; Ciais, P.; Peylin, P.; Huang, Y.; Sitch, S.; Wang, T. The Carbon Balance of Terrestrial Ecosystems in China. *Nature* **2009**, *458*, 1009–1013. [[CrossRef](#)] [[PubMed](#)]
16. Yu, G.; Chen, Z.; Piao, S.; Peng, C.; Ciais, P.; Wang, Q.; Li, X.; Zhu, X. High Carbon Dioxide Uptake by Subtropical Forest Ecosystems in the East Asian Monsoon Region. *Proc. Natl. Acad. Sci. USA* **2014**, *111*, 4910–4915. [[CrossRef](#)] [[PubMed](#)]
17. National Bureau of Statistics of China. *China Statistical Yearbook*; China Statistics Press: Beijing, China, 2022; ISBN 978-7-5037-9950-1.
18. Xu, K.; Zeng, H.; Zhang, Z.; Xie, J.; Yang, Y. Remote sensing analysis of correlation between forest growing season and temperature and precipitation in subtropical Fujian Province. *J. Geo-Inf. Sci.* **2015**, *17*, 1249–1259.
19. Niu, S.; Fu, Z.; Luo, Y.; Stoy, P.C.; Keenan, T.F.; Poulter, B.; Zhang, L.; Piao, S.; Zhou, X.; Zheng, H.; et al. Interannual Variability of Ecosystem Carbon Exchange: From Observation to Prediction. *Glob. Ecol. Biogeogr.* **2017**, *26*, 1225–1237. [[CrossRef](#)]
20. Sun, H.; Chen, Y.; Xiong, J.; Ye, C.; Yong, Z.; Wang, Y.; He, D.; Xu, S. Relationships between Climate Change, Phenology, Edaphic Factors, and Net Primary Productivity across the Tibetan Plateau. *Int. J. Appl. Earth Obs. Geoinf.* **2022**, *107*, 102708. [[CrossRef](#)]
21. Delpierre, N.; Vitasse, Y.; Chuine, I.; Guillemot, J.; Bazot, S.; Rutishauser, T.; Rathgeber, C.B.K. Temperate and Boreal Forest Tree Phenology: From Organ-Scale Processes to Terrestrial Ecosystem Models. *Ann. For. Sci.* **2016**, *73*, 5–25. [[CrossRef](#)]
22. Li, X.; Fu, Y.H.; Chen, S.; Xiao, J.; Yin, G.; Li, X.; Zhang, X.; Geng, X.; Wu, Z.; Zhou, X.; et al. Increasing Importance of Precipitation in Spring Phenology with Decreasing Latitudes in Subtropical Forest Area in China. *Agric. For. Meteorol.* **2021**, *304–305*, 108427. [[CrossRef](#)]
23. Fu, Y.H.; Zhao, H.; Piao, S.; Peaucelle, M.; Peng, S.; Zhou, G.; Ciais, P.; Huang, M.; Menzel, A.; Peñuelas, J.; et al. Declining Global Warming Effects on the Phenology of Spring Leaf Unfolding. *Nature* **2015**, *526*, 104–107. [[CrossRef](#)]
24. Du, Y.; Pan, Y.; Ma, K. Moderate Chilling Requirement Controls Budburst for Subtropical Species in China. *Agric. For. Meteorol.* **2019**, *278*, 107693. [[CrossRef](#)]
25. Park, J.Y.; Muller-Landau, H.C.; Lichstein, J.W.; Rifai, S.W.; Dandois, J.P.; Bohlman, S.A. Quantifying Leaf Phenology of Individual Trees and Species in a Tropical Forest Using Unmanned Aerial Vehicle (UAV) Images. *Remote Sens.* **2019**, *11*, 1534. [[CrossRef](#)]
26. Song, Z.; Song, X.; Pan, Y.; Dai, K.; Shou, J.; Chen, Q.; Huang, J.; Tang, X.; Huang, Z.; Du, Y. Effects of Winter Chilling and Photoperiod on Leaf-out and Flowering in a Subtropical Evergreen Broadleaved Forest in China. *For. Ecol. Manag.* **2020**, *458*, 117766. [[CrossRef](#)]
27. Li, Z.; Wang, R.; Liu, B.; Qian, Z.; Wu, Y.; Li, C. Responses of Vegetation Autumn Phenology to Climatic Factors in Northern China. *Sustainability* **2022**, *14*, 8590. [[CrossRef](#)]
28. Yuan, Y.; Bao, A.; Jiapaer, G.; Jiang, L.; De Maeyer, P. Phenology-Based Seasonal Terrestrial Vegetation Growth Response to Climate Variability with Consideration of Cumulative Effect and Biological Carryover. *Sci. Total Environ.* **2022**, *817*, 152805. [[CrossRef](#)] [[PubMed](#)]
29. Tang, W.; Liu, S.; Kang, P.; Peng, X.; Li, Y.; Guo, R.; Jia, J.; Liu, M.; Zhu, L. Quantifying the Lagged Effects of Climate Factors on Vegetation Growth in 32 Major Cities of China. *Ecol. Indic.* **2021**, *132*, 108290. [[CrossRef](#)]
30. Liu, N.; Shi, Y.; Ding, Y.; Liu, L.; Peng, S. Temporal Effects of Climatic Factors on Vegetation Phenology on the Loess Plateau, China. *J. Plant Ecol.* **2023**, *16*, rtac063. [[CrossRef](#)]
31. Wang, J.; Zhang, T.; Fu, B. A Measure of Spatial Stratified Heterogeneity. *Ecol. Indic.* **2016**, *67*, 250–256. [[CrossRef](#)]
32. Wang, J.; Xu, C. Geodetectors: Principles and prospects. *Acta Geogr. Sin.* **2017**, *72*, 116–134. [[CrossRef](#)]
33. Luo, L.; Mei, K.; Qu, L.; Zhang, C.; Chen, H.; Wang, S.; Di, D.; Huang, H.; Wang, Z.; Xia, F.; et al. Assessment of the Geographical Detector Method for Investigating Heavy Metal Source Apportionment in an Urban Watershed of Eastern China. *Sci. Total Environ.* **2019**, *653*, 714–722. [[CrossRef](#)]
34. Li, C.; Zou, Y.; He, J.; Zhang, W.; Gao, L.; Zhuang, D. Response of Vegetation Phenology to the Interaction of Temperature and Precipitation Changes in Qilian Mountains. *Remote Sens.* **2022**, *14*, 1248. [[CrossRef](#)]
35. Peng, H.; Xia, H.; Chen, H.; Zhi, P.; Xu, Z. Spatial Variation Characteristics of Vegetation Phenology and Its Influencing Factors in the Subtropical Monsoon Climate Region of Southern China. *PLoS ONE* **2021**, *16*, e0250825. [[CrossRef](#)]
36. Sun, Y.; Guan, Q.; Wang, Q.; Yang, L.; Pan, N.; Ma, Y.; Luo, H. Quantitative Assessment of the Impact of Climatic Factors on Phenological Changes in the Qilian Mountains, China. *For. Ecol. Manag.* **2021**, *499*, 119594. [[CrossRef](#)]
37. Yang, C.; Deng, K.; Peng, D.; Jiang, L.; Zhao, M.; Liu, J.; Qiu, X. Spatiotemporal Characteristics and Heterogeneity of Vegetation Phenology in the Yangtze River Delta. *Remote Sens.* **2022**, *14*, 2984. [[CrossRef](#)]
38. Zhan, Z. (Ed.) *Forest Site Types in China*; China Forestry Publishing: Beijing, China, 1995; ISBN 978-7-5038-1484-6.

39. Yang, Q.; Zheng, D.; Wu, S. Study on ecological areal system in China. *Prog. Nat. Sci.* **2002**, *12*, 65–69. [[CrossRef](#)]
40. Gray, J.; Sulla-Menashe, D.; Friedl, M.A. *User Guide to Collection 6 MODIS Land Cover Dynamics (MCD12Q2) Product*; NASA EOSDIS Land Processes DAAC: Missoula, MT, USA, 2019.
41. Ganguly, S.; Friedl, M.A.; Tan, B.; Zhang, X.; Verma, M. Land Surface Phenology from MODIS: Characterization of the Collection 5 Global Land Cover Dynamics Product. *Remote Sens. Environ.* **2010**, *114*, 1805–1816. [[CrossRef](#)]
42. Peng, D.; Zhang, X.; Wu, C.; Huang, W.; Gonsamo, A.; Huete, A.R.; Didan, K.; Tan, B.; Liu, X.; Zhang, B. Intercomparison and Evaluation of Spring Phenology Products Using National Phenology Network and AmeriFlux Observations in the Contiguous United States. *Agric. For. Meteorol.* **2017**, *242*, 33–46. [[CrossRef](#)]
43. Zhang, J.; Tong, X.; Zhang, J.; Meng, P.; Li, J.; Liu, P. Dynamics of Phenology and Its Response to Climatic Variables in a Warm-Temperate Mixed Plantation. *For. Ecol. Manag.* **2021**, *483*, 118785. [[CrossRef](#)]
44. Purdy, L.M.; Sang, Z.; Beaubien, E.; Hamann, A. Validating Remotely Sensed Land Surface Phenology with Leaf out Records from a Citizen Science Network. *Int. J. Appl. Earth Obs. Geoinf.* **2023**, *116*, 103148. [[CrossRef](#)]
45. Yang, L.; Wu, B.; Ma, J. Response of plant phenology to climate change in Fujian province. *Chin. Agric. Sci. Bull.* **2016**, *32*, 139–150. [[CrossRef](#)]
46. Yang, H.; Xiao, P.; Feng, X.; Li, H. Accuracy Assessment of Seven Global Land Cover Datasets over China. *ISPRS J. Photogramm. Remote Sens.* **2017**, *125*, 156–173. [[CrossRef](#)]
47. Peng, S.; Ding, Y.; Liu, W.; Li, Z. 1km Monthly Temperature and Precipitation Dataset for China from 1901 to 2017. *Earth Syst. Sci. Data* **2019**, *11*, 1931–1946. [[CrossRef](#)]
48. Li, B.; Pan, B.; Han, J. Discussion on basic landform types and their classification indexes in China. *Quat. Sci.* **2008**, *28*, 535–543.
49. Kendall, M.G. *Rank Correlation Methods*; Griffin: Oxford, UK, 1948; ISBN 0-19-520837-4.
50. Tošić, I. Spatial and Temporal Variability of Winter and Summer Precipitation over Serbia and Montenegro. *Theor. Appl. Clim.* **2004**, *77*, 47–56. [[CrossRef](#)]
51. Shi, S.; Wang, X.; Hu, Z.; Zhao, X.; Zhang, S.; Hou, M.; Zhang, N. Geographic Detector-Based Quantitative Assessment Enhances Attribution Analysis of Climate and Topography Factors to Vegetation Variation for Spatial Heterogeneity and Coupling. *Glob. Ecol. Conserv.* **2023**, *42*, e02398. [[CrossRef](#)]
52. Jia, L.; Yu, K.; Li, Z.; Ren, Z.; Li, H.; Li, P. Identification of Vegetation Coverage Variation and Quantitative the Impact of Environmental Factors on Its Spatial Distribution in the Pisha Sandstone Area. *Sustainability* **2023**, *15*, 6054. [[CrossRef](#)]
53. Zhang, Y.; Liu, X.; Jiao, W.; Wu, X.; Zeng, X.; Zhao, L.; Wang, L.; Guo, J.; Xing, X.; Hong, Y. Spatial Heterogeneity of Vegetation Resilience Changes to Different Drought Types. *Earth's Future* **2023**, *11*, e2022EF003108. [[CrossRef](#)]
54. Wang, M.; Wang, Y.; Li, Z.; Zhang, H. Analysis of Spatial-Temporal Changes and Driving Factors of Vegetation Coverage in Jiamusi City. *Forests* **2023**, *14*, 1902. [[CrossRef](#)]
55. Song, Y.; Wang, J.; Ge, Y.; Xu, C. An Optimal Parameters-Based Geographical Detector Model Enhances Geographic Characteristics of Explanatory Variables for Spatial Heterogeneity Analysis: Cases with Different Types of Spatial Data. *GIScience Remote Sens.* **2020**, *57*, 593–610. [[CrossRef](#)]
56. R Core Team. *R: A Language and Environment for Statistical Computing*; R Foundation Statistical Computing: Vienna, Austria, 2022.
57. Wen, Y.; Liu, X.; Xin, Q.; Wu, J.; Xu, X.; Pei, F.; Li, X.; Du, G.; Cai, Y.; Lin, K.; et al. Cumulative Effects of Climatic Factors on Terrestrial Vegetation Growth. *J. Geophys. Res. Biogeosci.* **2019**, *124*, 789–806. [[CrossRef](#)]
58. Wu, D.; Zhao, X.; Liang, S.; Zhou, T.; Huang, K.; Tang, B.; Zhao, W. Time-Lag Effects of Global Vegetation Responses to Climate Chang. *Glob. Chang. Biol.* **2015**, *21*, 3520–3531. [[CrossRef](#)] [[PubMed](#)]
59. Qiu, B.; Zhong, M.; Tang, Z.; Chen, C. Spatiotemporal Variability of Vegetation Phenology with Reference to Altitude and Climate in the Subtropical Mountain and Hill Region, China. *Chin. Sci. Bull.* **2013**, *58*, 2883–2892. [[CrossRef](#)]
60. Zhang, Y.; Yin, P.; Li, X.; Niu, Q.; Wang, Y.; Cao, W.; Huang, J.; Chen, H.; Yao, X.; Yu, L.; et al. The Divergent Response of Vegetation Phenology to Urbanization: A Case Study of Beijing City, China. *Sci. Total Environ.* **2022**, *803*, 150079. [[CrossRef](#)] [[PubMed](#)]
61. Colditz, R.R.; Lopez, G.; Maeda, P.; Cruz, I.; Ressler, R. Phenology and Phenological Variability of Mexican Ecosystems. In Proceedings of the 2009 IEEE International Geoscience and Remote Sensing Symposium, Cape Town, South Africa, 12–17 July 2009; pp. IV-1038–IV-1041.
62. Wang, H.; Wang, H.; Ge, Q.; Dai, J. The Interactive Effects of Chilling, Photoperiod, and Forcing Temperature on Flowering Phenology of Temperate Woody Plants. *Front. Plant Sci.* **2020**, *11*, 443. [[CrossRef](#)] [[PubMed](#)]
63. Mendoza, I.; Peres, C.A.; Morellato, L.P.C. Continental-Scale Patterns and Climatic Drivers of Fruiting Phenology: A Quantitative Neotropical Review. *Glob. Planet. Chang.* **2017**, *148*, 227–241. [[CrossRef](#)]
64. Ren, P.; Liu, Z.; Zhou, X.; Peng, C.; Xiao, J.; Wang, S.; Li, X.; Li, P. Strong Controls of Daily Minimum Temperature on the Autumn Photosynthetic Phenology of Subtropical Vegetation in China. *For. Ecosyst.* **2021**, *8*, 31. [[CrossRef](#)]
65. Ge, C.; Sun, S.; Yao, R.; Sun, P.; Li, M.; Bian, Y. Long-Term Vegetation Phenology Changes and Response to Multi-Scale Meteorological Drought on the Loess Plateau, China. *J. Hydrol.* **2022**, *614*, 128605. [[CrossRef](#)]
66. De Frenne, P.; Lenoir, J.; Luoto, M.; Scheffers, B.R.; Zellweger, F.; Aalto, J.; Ashcroft, M.B.; Christiansen, D.M.; Decocq, G.; De Pauw, K.; et al. Forest Microclimates and Climate Change: Importance, Drivers and Future Research Agenda. *Glob. Chang. Biol.* **2021**, *27*, 2279–2297. [[CrossRef](#)]

67. Davidson, E.A.; de Araújo, A.C.; Artaxo, P.; Balch, J.K.; Brown, I.F.; Bustamante, M.M.C.; Coe, M.T.; DeFries, R.S.; Keller, M.; Longo, M.; et al. The Amazon Basin in Transition. *Nature* **2012**, *481*, 321–328. [[CrossRef](#)]
68. Brando, P.M.; Goetz, S.J.; Baccini, A.; Nepstad, D.C.; Beck, P.S.A.; Christman, M.C. Seasonal and Interannual Variability of Climate and Vegetation Indices across the Amazon. *Proc. Natl. Acad. Sci. USA* **2010**, *107*, 14685–14690. [[CrossRef](#)]
69. Shen, M.; Piao, S.; Cong, N.; Zhang, G.; Jassens, I.A. Precipitation Impacts on Vegetation Spring Phenology on the Tibetan Plateau. *Glob. Chang. Biol.* **2015**, *21*, 3647–3656. [[CrossRef](#)] [[PubMed](#)]
70. Lang, G.A.; Early, J.D.; Martin, G.C.; Darnell, R.L. Endo-, Para-, and Ecodormancy: Physiological Terminology and Classification for Dormancy Research. *HortScience* **1987**, *22*, 371–377. [[CrossRef](#)]
71. Chuine, I.; Bonhomme, M.; Legave, J.-M.; García de Cortázar-Atauri, I.; Charrier, G.; Lacoite, A.; Améglio, T. Can Phenological Models Predict Tree Phenology Accurately in the Future? The Unrevealed Hurdle of Endodormancy Break. *Glob. Chang. Biol.* **2016**, *22*, 3444–3460. [[CrossRef](#)] [[PubMed](#)]
72. Garrigues, R.; Dox, I.; Flores, O.; Marchand, L.J.; Malyshev, A.V.; Beemster, G.; AbdElgawad, H.; Janssens, I.; Asard, H.; Campioli, M. Late Autumn Warming Can Both Delay and Advance Spring Budburst through Contrasting Effects on Bud Dormancy Depth in *Fagus sylvatica* L. *Tree Physiol.* **2023**, *43*, tpad080. [[CrossRef](#)] [[PubMed](#)]
73. Li, J.; Huang, J.-G.; Tardif, J.C.; Liang, H.; Jiang, S.; Zhu, H.; Zhou, P. Spatially Heterogeneous Responses of Tree Radial Growth to Recent El Niño Southern-Oscillation Variability across East Asia Subtropical Forests. *Agric. For. Meteorol.* **2020**, *287*, 107939. [[CrossRef](#)]
74. Prior, L.D.; Bowman, D.M.J.S.; Eamus, D. Seasonal Differences in Leaf Attributes in Australian Tropical Tree Species: Family and Habitat Comparisons. *Funct. Ecol.* **2004**, *18*, 707–718. [[CrossRef](#)]
75. Gong, F.; Chen, X.; Yuan, W.; Su, Y.; Yang, X.; Liu, L.; Sun, Q.; Wu, J.; Dai, Y.; Shang, J. Partitioning of Three Phenology Rhythms in American Tropical and Subtropical Forests Using Remotely Sensed Solar-Induced Chlorophyll Fluorescence and Field Litterfall Observations. *Int. J. Appl. Earth Obs. Geoinf.* **2022**, *107*, 102698. [[CrossRef](#)]
76. Cong, N.; Wang, T.; Nan, H.; Ma, Y.; Wang, X.; Myneni, R.B.; Piao, S. Changes in Satellite-Derived Spring Vegetation Green-up Date and Its Linkage to Climate in China from 1982 to 2010: A Multimethod Analysis. *Glob. Chang. Biol.* **2013**, *19*, 881–891. [[CrossRef](#)]

Disclaimer/Publisher’s Note: The statements, opinions and data contained in all publications are solely those of the individual author(s) and contributor(s) and not of MDPI and/or the editor(s). MDPI and/or the editor(s) disclaim responsibility for any injury to people or property resulting from any ideas, methods, instructions or products referred to in the content.